Western Kentucky University
TopSCHOLAR®

Masters Theses & Specialist Projects | Graduate School

5-2011

Determining the Ion-exchange Mechanism of Strontium into a Niobium Doped Titanosilicate

Samantha Jane Kramer
Western Kentucky University, samanthajkramer@gmail.com

Follow this and additional works at: http://digitalcommons.wku.edu/theses

 Part of the Environmental Chemistry Commons, Environmental Indicators and Impact Assessment Commons, and the Geochemistry Commons

Recommended Citation
Kramer, Samantha Jane, "Determining the Ion-exchange Mechanism of Strontium into a Niobium Doped Titanosilicate" (2011). *Masters Theses & Specialist Projects*. Paper 1068.
http://digitalcommons.wku.edu/theses/1068

This Thesis is brought to you for free and open access by TopSCHOLAR®. It has been accepted for inclusion in Masters Theses & Specialist Projects by an authorized administrator of TopSCHOLAR®. For more information, please contact topscholar@wku.edu.

DETERMINING THE ION-EXCHANGE MECHANISM OF STRONTIUM INTO A NIOBIUM DOPED TITANOSILICATE

A Thesis
Presented to
The Faculty of the Department of Geography and Geology
Western Kentucky University
Bowling Green, Kentucky

In Partial Fulfillment
Of the Requirements for the Degree
Master of Science

By
Samantha Jane Kramer

May 2011

DETERMINING THE ION-EXCHANGE MECHANISM OF STRONTIUM INTO A NIOBIUM DOPED TITANOSILICATE

Date Recommended may 23, 2011

Aaron J. Celestian, Director of Thesis

Les Pesterfield

Andrew Wulff

Michael May

Richard G. Bowker June 7, 2011

Dean, Graduate Studies and Research Date

To my family for never ceasing to remind me I had a thesis to finish, to Josh for his support and love, and finally to my advisor and inspiration Dr. Aaron Celestian for his abounding patience and reassurance that research can be successful even if you don't achieve what you set out to do.

And I thank Dr. C's wife, Jen, too for keeping us all calm and being so supportive.

Thank you all.

TABLE OF CONTENTS

List of Figures ……. v
List of Tables ……... vi
Abstract …… vii
Chapter 1 Introduction …… 1
I. Microporous Materials: Zeolites ……..... 1
II. Heterosilicates: the Zeolitic Materials …….. 5
III. Ion Exchange …… 7
IV. Applications of Ion Exchange Materials …….. 12
V. The Titanosilicate ……. 14
Chapter 2 Experimental Methods …….. 29
I. Material Synthesis …… 29
II. Time Resolved Ion Exchange …….. 30
III. Analysis …… 32
Chapter 3 Results and Discussion …….. 34
I. X-ray Diffraction and Phase Transitions ……. 34
II. Rietveld Structure Refinements ……... 39
Strontium position and symmetry changes 43
Strontium occupancy and mechanism 48
Chapter 4 Conclusions …… 50
Appendix ……..……... 52
A. Atomic Positions of H-NbTS, as refined 52
B. Atomic Positions of Sr-NbTS, as refined 53
C. Bond Valence Sum Calculations 54
References ……... 57

LIST OF FIGURES

Figure 1: *Tetrahedral framework and charge balancing*..... 3
Figure 2: *Natrolite*..... 4
Figure 3: *Sitinakite* 6
Figure 4: *Stoichiometric exchange* 8
Figure 5: *Double lever mechanism* 11
Figure 6: *Sodium titanosilicate with sitinakite topology* 16
Figure 7a: *Hydrogen titanosilicate* 18
Figure 7b: *Expanded view of H-TS* 19
Figure 8: *Sodium exchanged TS, NaH-TS* 21
Figure 9: *Cesium exchanged TS, Cs-TS* 23
Figure 10: *Potassium exchanged TS, KH-TS* 25
Figure 11a: *Strontium exchanged TS, in Cmmm* 27
Figure 11b: *Strontium exchanged TS, in $P4_2/mmc$* 27
Figure 12: *Polyimide environmental cell* 31
Figure 13: *Time resolved diffraction data for Exp B* 35
Figure 14a: *ITTFA plot of Exp B* 37
Figure 14b: *ITTFA plot of Exp C* 38
Figure 15: *Diffraction pattern of H-NbTS* 40
Figure 16: *Models of H-NbTS* 41
Figure 17: *Models of SrH-NbTS* 44
Figure 18: *Relationship from $P4_2/mcm$ to P-42m* 45
Figure 19: *Bond geometry for SrH-NbTS* 47
Figure 20: *Strontium occupancy vs. frame number*..... 49

LIST OF TABLES

Table 1: *Common Ion Exchange Applications* ……... 12
Table 2: *Unit cell parameters of the sodium phase titanosilicate and the protonated phase titanosilicate* …….…….…. 20
Table 3*: Refinement parameters of H-NbTS and SrH-NbTS* ……. 43
Table 4: *Strontium-oxygen interatomic distances (Å) in SrNbTS* ……... 46

DETERMINING THE ION-EXCHANGE MECHANISM OF STRONTIUM INTO A NIOBIUM DOPED TITANOSILICATE

Samantha Jane Kramer May 2011 58 Pages

Directed by: Aaron Celestian, Michael May, Andrew Wulff, and Les Pesterfield

Department of Geography and Geology Western Kentucky University

A 25% niobium substituted sitinakite was exchanged with strontium as time resolved X-ray diffraction data was collected. The structural modeling of this data by Rietveld method[1] has lead to the determination of the atomic positions of the ions and unit cell parameters as strontium occupancy increases.

The starting material of the exchange experiment is the protonated phase, $H_2Nb_{0.67}Ti_{1.33}SiO_7 \cdot 1.9\ H_2O$, with space group $P4_2/mcm$[2,3]. Once strontium (Sr^{2+}) enters the unit cell, extra-framework H_2O molecules shift to provide the necessary hydration coordination. These new positions of H_2O result in a lowering of symmetry to the P-42m space group, and it is thought that the new hydrogen bonding network serves to enhance strontium ion diffusion into the channels of sitinakite. Exchange of strontium into the microporous material reaches a maximum fractional occupancy of 21% when a 10.0 mM strontium ion solution is forced over the powdered material. Sequestration of strontium into this material has contributed valuable information to the study of microporous materials and ion exchange chemistries.

Chapter 1

INTRODUCTION

I. Microporous Materials: Zeolites

Of all the materials found naturally on Earth, those having absorbent properties, or the ability to readily and selectively absorb mobile constituents, may be the most interesting; urging scientists to push the bounds of creativity and synthesize new materials to incorporate the desired chemical properties. The term microporous adequately describes these absorbent materials as well as one specific grouping, known as zeolites. Zeolites are more thoroughly defined as microporous crystalline aluminosilicates and are among the most common authigenic silicate minerals found in sedimentary deposits and deposits from hydrothermal veins[4].

The term zeolite was first introduced in 1756 by Baron Axel Fredrik Cronstedt, a Swedish chemist also credited with the discovery of nickel and tungsten[5]. In his examination of the mineral stilbite, he observed that the stone appeared "to boil" upon heating[6], providing the name from the Greek, zeo – (to boil) and lithos – (stone). Cronstedt also found that the rehydration and subsequent "re-boiling" of the material demonstrated another important property of most zeolites, the reversible absorption of molecules and ions.

Zeolites, by definition, consist of a framework of AlO_4 - and SiO_4 – tetrahedron (Figure 1). The framework carries an anionic charge due to the inclusion of the Al^{3+} ions and must be charge balanced by interstitial cations such as sodium (Na^+) or potassium (K^+)[7]. Water molecules are commonly found interstitially and provide useful hydrogen-bonding. This, in itself, does not differentiate zeolites from other silicate minerals. The

unique geometry in which these tetrahedrons bind together creates a system of interconnecting channels, ultimately resulting in the microporous framework that is important to zeolites and ion exchange reactions; such channels range in size from 1 Å to 20 Å in diameter[8]. It is the combination of uniformity in the channels and the negative charge of the framework that allows the interstitial cations and molecules to be exchanged or diffused through the material, sometimes reversibly (Figure 2). Early in the twentieth century, studies in the adsorption of organic gases by McBain[9] recognized the potential of separating ions and molecules by zeolites, and the coining of the term "molecular sieves."

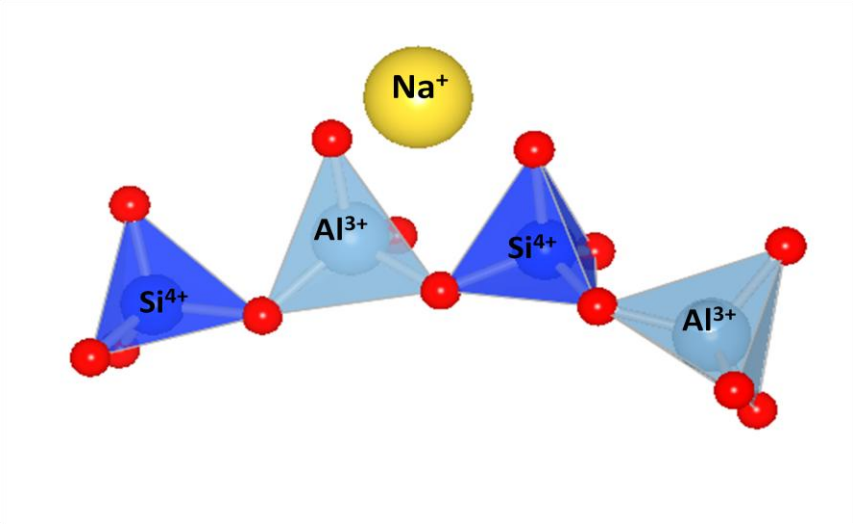


Figure 1: *Aluminum and silica tetrahedrons with a sodium ion to help balance the anionic framework. As noted in the figure, Si is represented in darker blue, Al in the lighter blue, Na in yellow, and oxygen in red.*

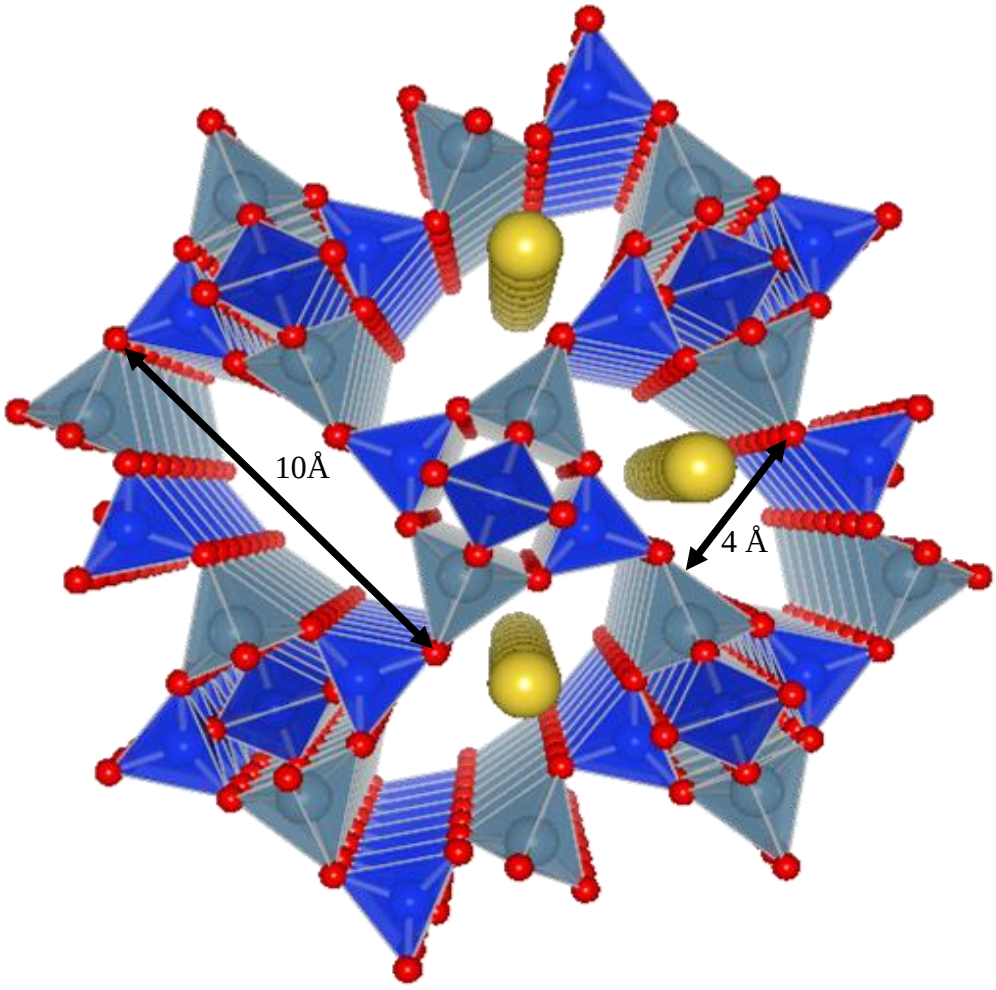


Figure 2: *Natrolite as seen along the crystallographic c-axis. This zeolite is an excellent example of uniform microporous structure. The framework is entirely comprised of SiO_4 and AlO_4 tetrahedrons, shown here as blue and gray polyhedrons respectively with oxygen shown in red. While pore sizes in zeolites can range from 1 Å – 20 Å in diameter, natrolite has a channel oriented along the c-axis that is approximately 4 Å by 10 Å. Some of the interstitial Na^+ (yellow) have been removed for simplicity.*

II. Heterosilicates: the Zeolitic Materials

The term zeolite refers to a specific group of materials whose frameworks contain only Al and Si metals, or more strictly speaking, frameworks of only tetrahedrons[4]. However substitutions in various metal sites do occur. The interconnected pathways of channels are still present in uniform geometries, so these materials are *zeolitic*, while not being actually zeolites. These materials have been termed *heterosilicates*, having both octahedral and tetrahedral framework metal sites. Typically the SiO_4 and AlO_4 – tetrahedrons are polymerized into chains, layers, or groups of chains with isolated octahedrons between[10]. This produces typical T:M ratios (tetrahedral to octahedral metals) of 1.6 – 8.0. In more rare instances, minerals like sitinakite, koarovite, and baotite, the T:M ratio is < 1.0; there are more octahedral metal sites than SiO_4 - tetrahedron sites[10]. (Figure 3) This factor greatly affects the structural chemistry of the material. More significant to this study is that the lower the T:M ratio, the more negatively charged the framework becomes, more interstitial cations are required to reach a charge balance (i.e.: a higher exchange capacity).

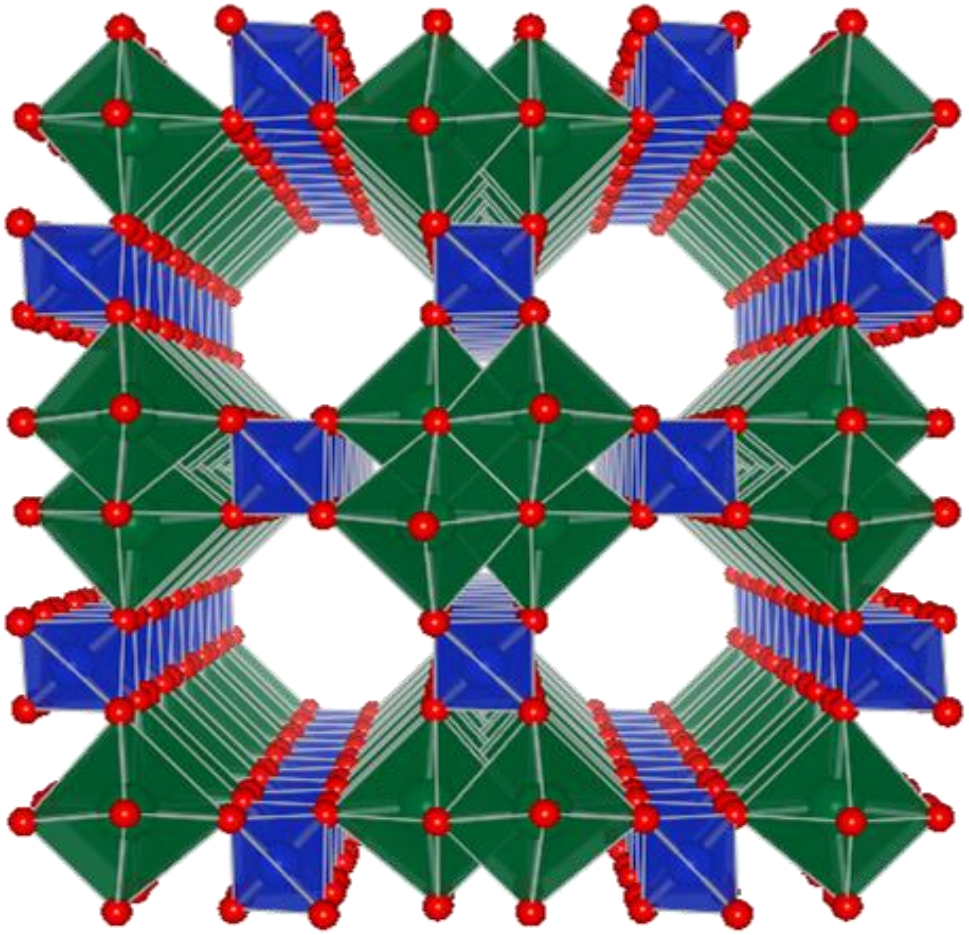


Figure 3: *Sitinakite as seen along the crystallographic c-axis. No interstitial ions have been shown to better view the channels. This heterosilicate exhibits the uniform porous channel structure, while being composed of both octahedra and tetrahedra. SiO_4 tetrahedra, shown in blue, bind to the green TiO_6 octahedra towers, with oxygen shown in red. The channels are just over 6 Å in diameter.*

III. Ion Exchange

In certain instances, ion species can be readily replaced by other available ionic species. Ideally this replacement or exchange occurs between a stationary phase (crystalline material) and mobile phase (electrolyte solution). The stationary phase is often called an exchanger, and must contain ions capable of being readily exchanged for ions in the mobile phase. Ion exchange differs from a process known as sorption, even if both involve a dissolved species moving in and around a solid. In ion exchange for every ion removed from the solution and taken up by the exchange material a stoichiometrically equivalent number of ions are released from the material into the solution. In sorption, the solute ions are non-stoichiometrically taken up without being replaced. This is the case whether the process is absorption, where ions are taken up within the bulk of the material, or adsorption, when ions adhere to the outer surfaces of the material[11]. The stoichiometric process of exchanging ions is necessary to balance the negatively charged framework of the material, i.e. zeolites. The competition of two or more ions for functional sites and the stoichiometric character of ion exchange is illustrated in Figure 4. As long as the exchanged quantities are charged-balanced the framework chemistry can be satisfied. This process may be reversable or not depending on framework chemistry and which phase is most thermodynamically stable or kinetically viable.

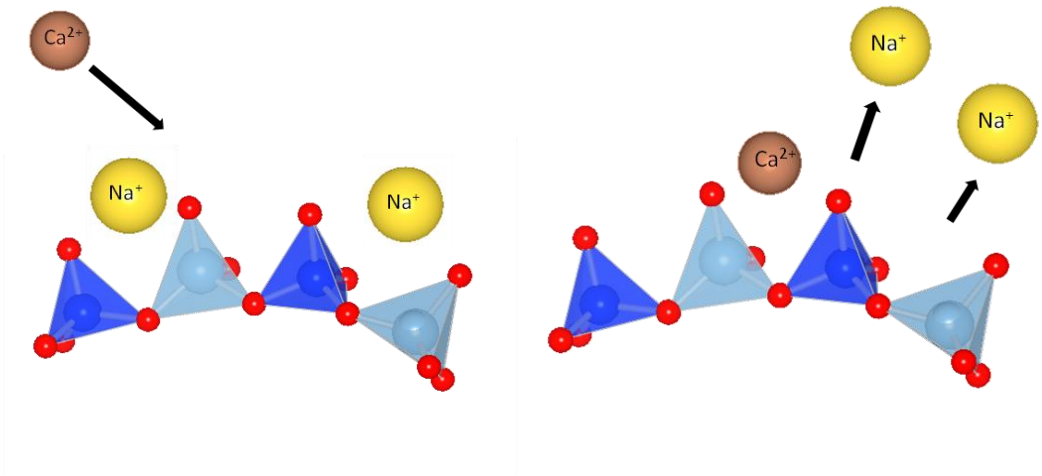


Figure 4: *Stoichiometric exchange of ions. SiO_4/AlO_4 tetrahedral frameworks are charged balanced by interstitial cations. In this instance one Ca^{2+} is exchanging for two Na^{+}, meeting the charge balance requirement of this segment of a crystalline solid.*

Many types of materials have been used in ion exchange processes; examples being clay minerals, synthetic gels, and inorganic resins (polymers). One of the earliest references of ion exchange can be found in Exodus 15:23, when logs were used to desalinate drinking water. Cellulose is known to be a decent exchanger of Mg^{2+}.[12] The first modern description is credited to two English chemists in the mid-nineteenth century[13] with the observation of cations being exchanged between a solution and certain types of soils. The chemical and structural make-up of an exchanger is a determinant of the specificity of the ions exchanged and its exchange capacity.

Molecular sieves, such as zeolitic materials, have a uniform channel structure and the framework chemistry to allow diffusion of ions and molecules through its bulk. The ease in which ions and molecules can be exchanged may give the impression that the process is disordered and chaotic. Structural determinations over the last several decades have demonstrated that ion exchange occurs in very definite sites within the lattice framework[8]. The complexity of some exchange pathways only reveals how much more there is to discover. As an example, the sequestration of cesium ions (Cs^+) into the protonated phase of synthetic sitinakite (H-TS) has been described as a 'double lever mechanism,[14] due to the two-step process observed from the diffusion.

Study of *in situ* X-ray diffraction and neutron diffraction data suggests that as Cs enters the Cs2 site of the H-TS a conformational change occurs, opening the channel to accept Cs into the Cs1 site [2,14,15]. (See Figure 5) The Cs2 site fills and the repulsive forces between Cs^+ and the dipole of the interstitial H_2O molecules causes the H_2O molecule to rotate $\approx 159^o$ and bond with Cs^+ in site Cs2. This hydration forces the H of the H_2O molecule close to the hydroxyl group attached to the Ti octahedron of the

framework; the response is then for the hydroxyl groups to bend away pulling the Ti octahedron with it by ≈5.8^{o}. The channel becomes less elliptical and the more preferred site (Cs1) is now available to be filled.

The ionic species must physically fit into the channel and the presence or absence of other interstitial ions and molecules has a profound impact on the effectiveness of a material as a selective ion exchanger. Additional examples will be discussed later on.

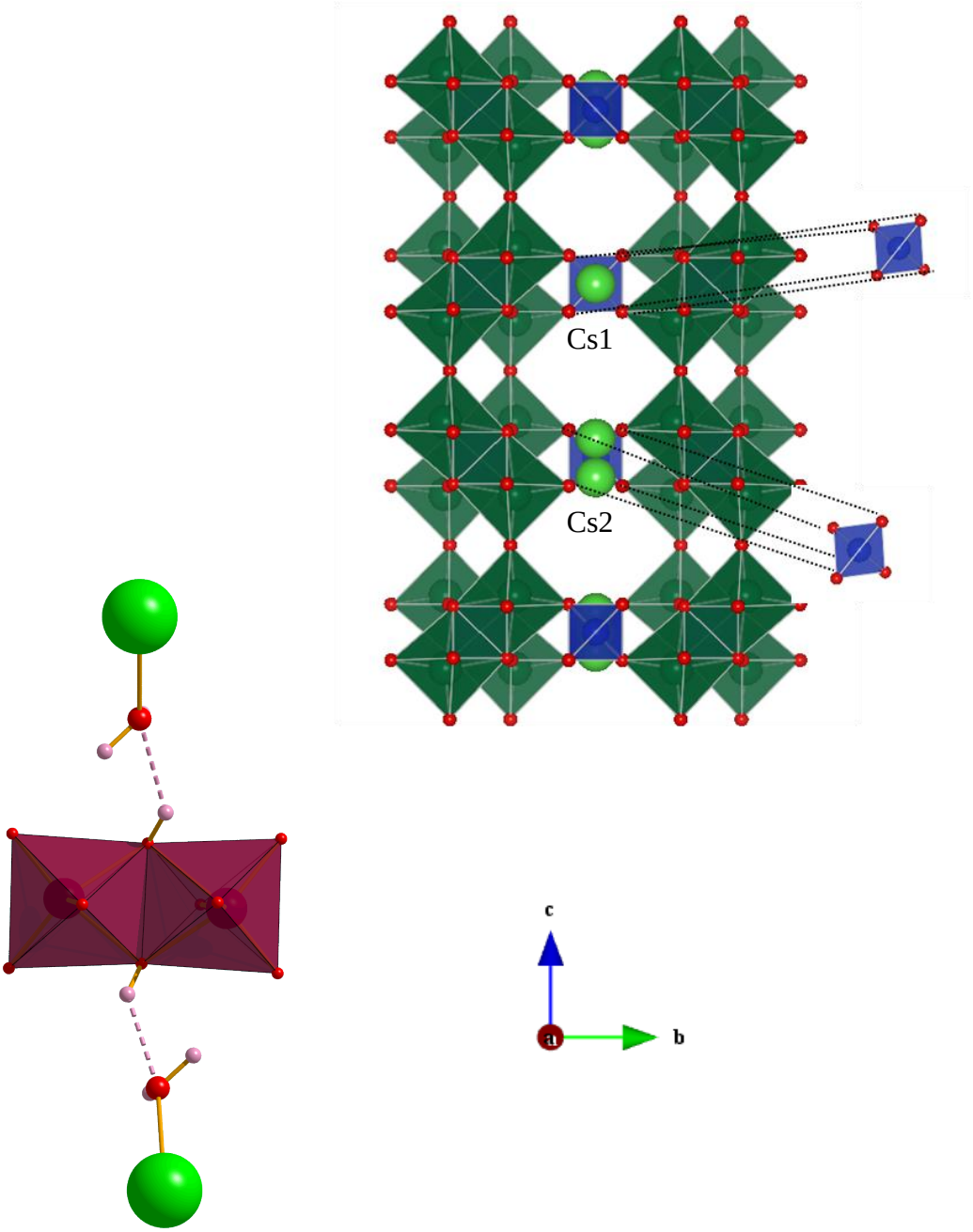


Figure 5: *Double lever mechanism as described by Celestian et al*[14] *and a model of the Cs positions within H-TS as seen along the ab plane.*

IV. Applications of Ion Exchange Materials

The property of ion exchange has been used for centuries by humans to purify drinking water, even if we did not understand the process that was taking place. Only recently has science begun to synthesize materials with the goal of harnessing the unique ion exchange capabilities of their natural analogues,[16] or to generate new materials for designer selectivity. Ion selective materials have been applied to purification processes in a variety of industrial fields and can be used for a variety of matrices (aqueous solutions, organic solvents, and even gases)[17]. There is a wealth of information with both current and potential applications of ion exchange materials[4,9,11-13,17]. See Table 1for a brief listing of applications[11]. To be most effective the right material must be selected for the matrices and constituents involved.

Table 1: Common Ion Exchange Applications[11]

Food and Pharmaceutical	Purification of amino acids, proteins, enzymes, and antibodies Controlled drug release Taste masking, odor masking
Analytical	Ion chromatography, desiccation
Water	Purification of potable drinking water Removal of heavy metals, nitrates, ammonia Preparation of deionized water, ultra pure water
Industrial	Petroleum refining, metal separation, treatment of effluent wastes
Environmental	Stream recovery, acid mine drainage, metal recovery Soil remediation Radioactive species recovery
Nuclear	Separation of Uranium and Rare Earth Metals Waste treatment and storage

The topic of nuclear waste disposal is of due importance when the lasting implications to environmental health are so dire. Past use of radioactive materials in government defense activities, power plants, and in medical and industrial research has produced large quantities of radioactive wastes that require permanent and safe disposal. Treatment of the nuclear wastes may help to render them less hazardous to allowing safer handling and storage, and potentially reducing the volume of radioactively contaminated waste.

The radioactive byproducts of nuclear reactions are generally present in waste solutions at low concentrations (10^{-3} to 10^{-5} Molarity), and the waste itself has a high salinity and typically high pH [3,18-21]. All materials in contact with byproduct waste solutions must meet several requirements to insure stability and safety if utilized in the treatment and storage. The first concern is of the intense radiation and heat generated by the many byproducts of uranium decay; materials must be resistant to these destabilizing affects. The isotopes ^{90}Sr and ^{137}Cs are among the most prevalent and most biologically hazardous byproducts , being γ-emitters with approximate 30 year half-lives [19]. Inorganic materials are better able to resist corrosion caused by the radiation and thermal influences of nuclear wastes. Secondly, the material must be highly selective to sequester the targeted species (like Sr and Cs) over the less toxic species like Na or K. Specific channel geometries and framework chemistries must be in place to facilitate targeted sequestration. A third concern in determining the suitability of an ion exchange material is its long term stability when exposed to high temperatures. Thermal stresses can cause extra-framework H_2O molecules to evaporate and cations to hydrolyze any remaining water molecules to form metal hydroxides or oxides. The available proton then forms a

hydroxyl group with framework oxygens, thus destroying the crystal structure[8]. Loss of structure integrity may lead to leaching of the entombed constituents, rendering a material unsuitable for long term storage.

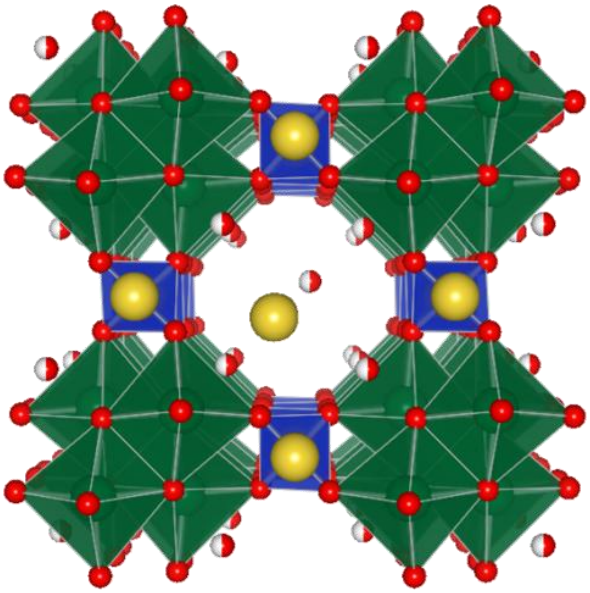
Techniques to prevent materials from leaching sequestered ions back into the environment have been developed and studied[22,23]. One such technique, cement encapsulation of zeolites, was deemed suitable for 'long term storage' when entombing ^{137}Cs in mixtures of clinoptilolite and chabazite minerals and clinoptilolite and mordenite tuff[24]. The exchanged zeolite materials are mixed with Portland cement and aggregate and solidified. The hardened blocks can be safely stored and transported, while exhibiting an impermeable surface.

V. The Titanosilicate

One particular material, sitinakite, has been shown to be successful in removing Cs and Sr ions from aqueous phases. It is easily synthesized in the lab and meets all requirements for a thermally stable, inorganic, selective ion exchanger [3,18-20]. Sitinakite can be found in the mines of Northern Russia where it was formed by the reaction of thermal ground water and the country rock[25]. Its name lends a good indication as to its main components, Si, Ti, Na, and K. This heterosilicate exhibits the zeolitic properties of being a reversible ion exchanger, even when framework atoms have been substituted out[25]. Studies have been conducted on the analogous structures of sitinakite since the early 1990s when an article published in *Waste Management* reported the effective sequestration of radioactive byproducts from nuclear wastes[18].

The synthetic material crystallizes with sitinakite topology, ideally posing a tetragonal space group of $P4_2/mcm$ and unit cell parameters of a = 7.832 Å and c = 11.945 Å [20]. Four edge-shared metal octahedra form cubane-like clusters, where two octahedra reside next to each other on one plane with two more residing just below, rotated at 90°. These cubane-like clusters are connected to each other in the *ab* plane by SiO_4 tetrahedra and in the *c* direction by the apical framework oxygens, as seen in Figure 6. Most often the metal octahedra are comprised of Ti-O, however partial substitution with Nb-O has been studied, as will be discussed later. The negatively charged framework encompasses one-dimensional channels running along the *c* direction (viewed as an 8-member ring, 8MR), and is neutralized by counter cations residing within the channels (Na^+). Perpendicular to the channels are vacancies in the faces of the four side walls of the channel. During synthesis the center of this vacancy is occupied with Na ions in six coordination (6-CN) with more Na^+ filling the channel.

i.



ii.

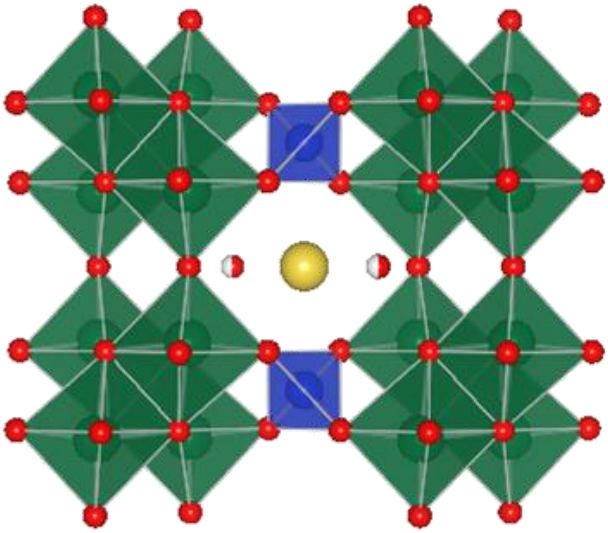


Figure 6: *Sodium titanosilicate (Na-TS) with basic sitinakite topology, $P4_2/mcm$. Seen along the* c*-axis (i) and along the* a*-axis (ii)*[26]*. The 8-member ring (8MR)is shown in (i) along* c *and a 6-member ring (6MR) along the* a *direction is shown in (ii). Ti = green, Si = blue, O = red, and Na = yellow, interstitial H_2O = red/white.*

Work has been done to optimize the synthesis of the titanosilicate and to study the various precursors that appear during synthesis like sodium nonatitanate (known as SNT)[15,27,28]. Ion exchange studies with the alkali metals (Na^+, K^+, and Cs^+) have been conducted in the protonated structure, H-TS[26]. Here the sodium titanosilicate (Na-TS as synthesized) was washed exhaustively with 1 M hydrochloric acid solutions, exchanging Na^+ with H^+. Neutron diffraction techniques were used to determine the locations of the newly exchanged protons[19]. The acid protons are bonded to the framework oxygens of the cubane-like clusters and are not present as H_3O^+. (See Figure 7a and 7b) The positioning of H^+ enforces the significance of exchange between specific atomic sites. After the exchange the unit cell dimensions alter, having space group $P4_2/mbc$. The new *a*-axis is the diagonal of the *ab* plane of the Na-TS, and the structure distorts to form an elliptical 8MR.

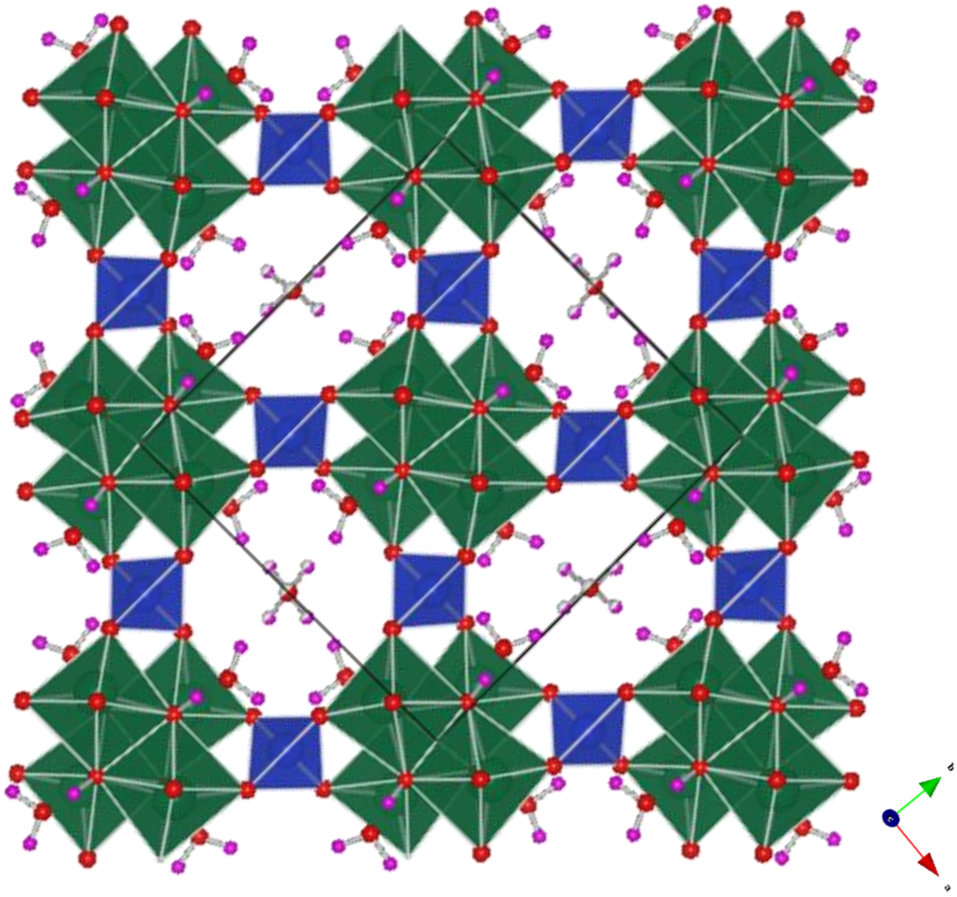


Figure 7a: *The H-TS framework, $P4_2/mbc$, as seen from the c-axis*[15]*. Notice the now elliptical 8MR in this collapsed, or exchanged, form. H = pink and pink/white, unit cell = black line.*

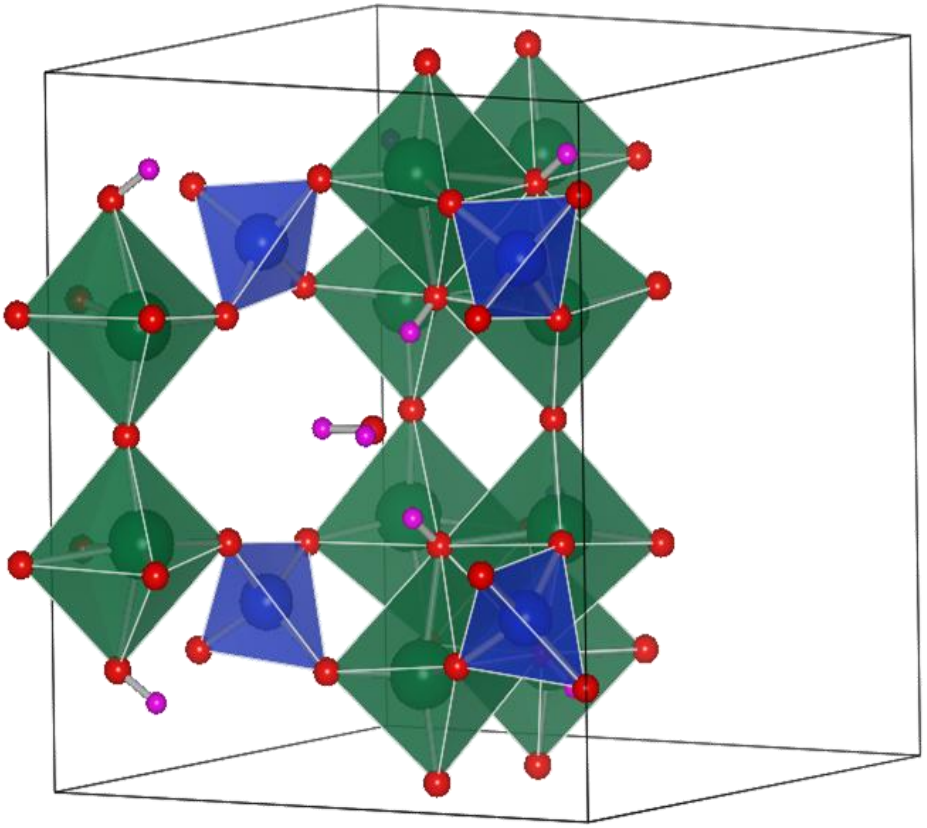


Figure 7b: *A portion of the H-TS framework, $H_2Ti_2O_3SiO_4 \cdot 2H_2O$, showing the location of the acid protons as bonded to the framework apical oxygens, and interstitial H_2O. O = red, H = pink, unit cell = black lines.*

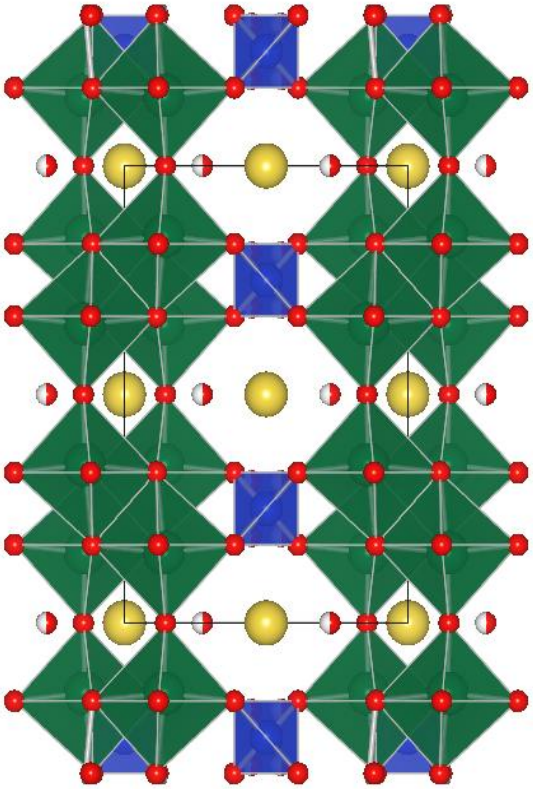
The protonated phase has shown to be more conducive to exchanging the larger alkali ions. This has been explained by the theorized existence of conjugated p_π - d_π orbitals in the O-Ti-O-Si-O bonds[29]. The conjugation (overlapping of electron orbitals) redistributes electron density lessening the negative charge on the oxygen atoms of the hydroxyl groups, and making the loss of the H^+ more feasible. It could also be that the H^+ is bonded to the oxygens that are bridging three Ti^{4+} ions and the electrostatic field of the metal ions repels the proton making it more easily ionizable.

***Table 2:** Unit cell parameters of the sodium titanosilicate and the protonated titanosilicate.*

	NaH-TS[26]	**H-TS[26]**
Formula	$Na_{1.64}H_{0.36}Ti_2O_3SiO_4 \cdot 1.8H_2O$	$H_2Ti_2O_3SiO_4 \cdot 1.5H_2O$
Space Group	$P4_2/mcm$	$P4_2/mbc$
a	7.832	11.039
c	11.945	11.886

Summarized by Clearfield et al. in 2006, the protonated TS (H-TS) effectively has three exchange sites; one within the framework (center of the 6MR), one near the framework at (c = 0, ½), and one in the center of the channel, 8MR (c = ¼, ¾)[20,26,27]. In the case of the Na^+, when exchanged into the protonated phase (H-TS) at half occupancy, $NaHTi_2O_3SiO_4 \cdot 2H_2O$, the unit cell reverts back to the initial space group (*$P4_2/mcm$*). The Na^+ preferentially enters the framework site, within the 6MR, supporting the structure and reverting the space symmetry (see Figure 8). The Na-O bond distances were very similar to those in the fully exchanged structure[20], and in the original synthesis.

View along *ab* plane



View along *c* axis

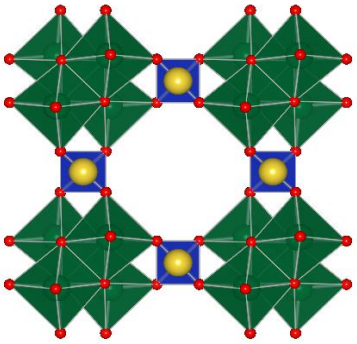


Figure 8: *NaH-TS, generated from the exchange of the H-TS material. Na^+ preferentially enters the framework site, the center of the 6MR, seemingly underneath the SiO_4 tetrahedra when viewed along the c-axis. Interstitial H_2O molecules have not been shown for clarity.*

When the H-TS is exchanged with Cs^+, the ions enter the center of the channel in two sites. One site is within the window of the 8MR itself and the other is just outside this window but still in the center of the channel. The close proximity of these two Cs sites makes simultaneous occupancy impossible; one site may fill per void. This is explained earlier by the "double-lever mechanism" of Celestian et al.[2] and is illustrated in Figure 5. The entry of Cs is analogous to that of Na in that Cs forces the structure into the $P4_2/mcm$ space group. Maximum occupancy is 25% of each site, with the remaining framework charge being neutralized by the acid protons. However, Na can still enter into the framework sites when the simultaneous exchange of Na^+ and Cs^+ is performed[30]. Figure 9 illustrates the atomic position of Cs within the channels.

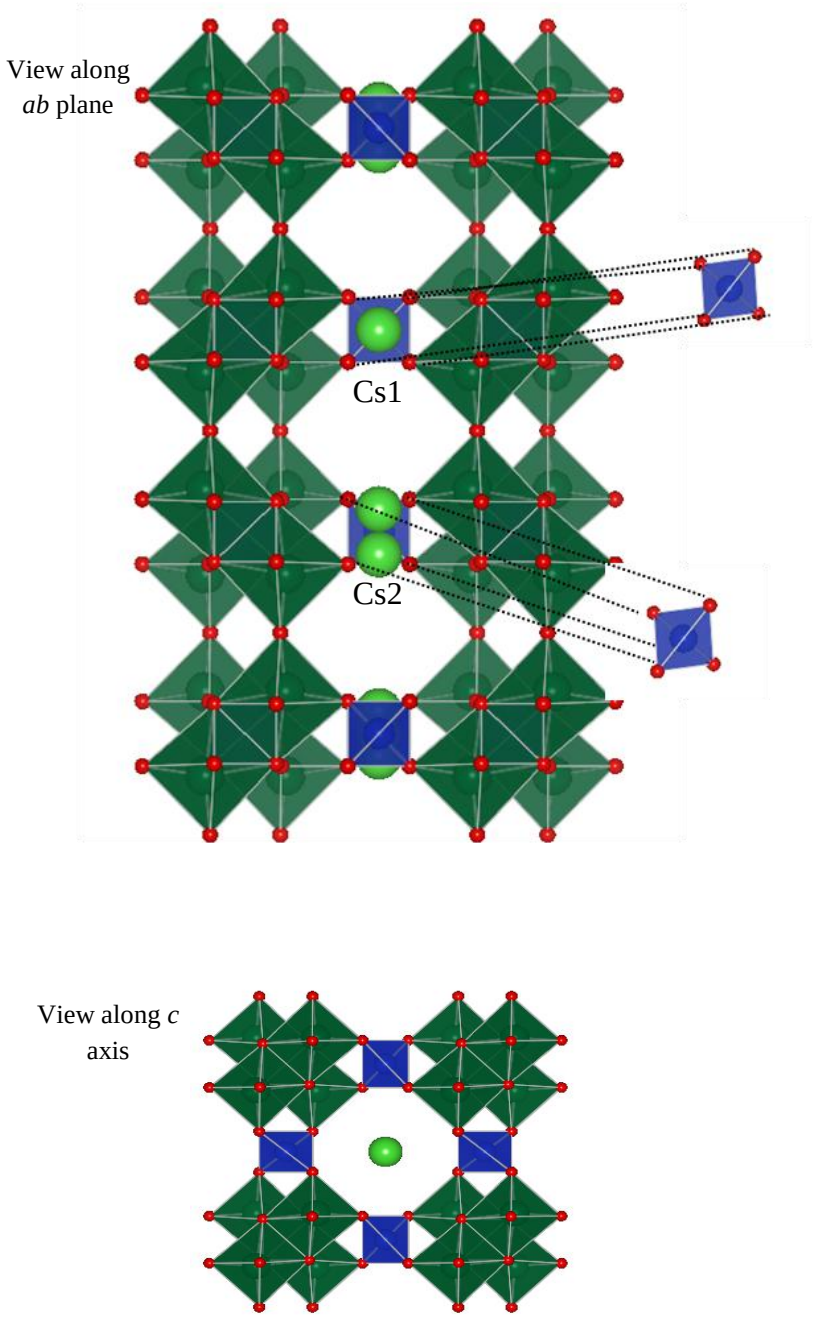
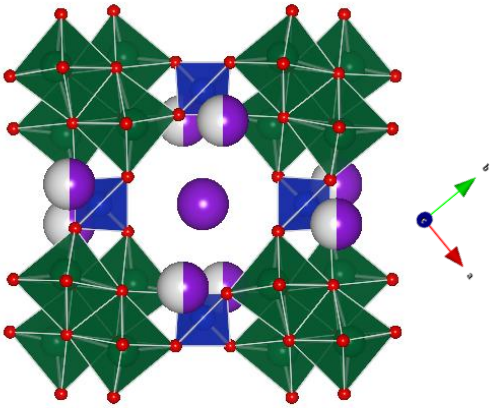


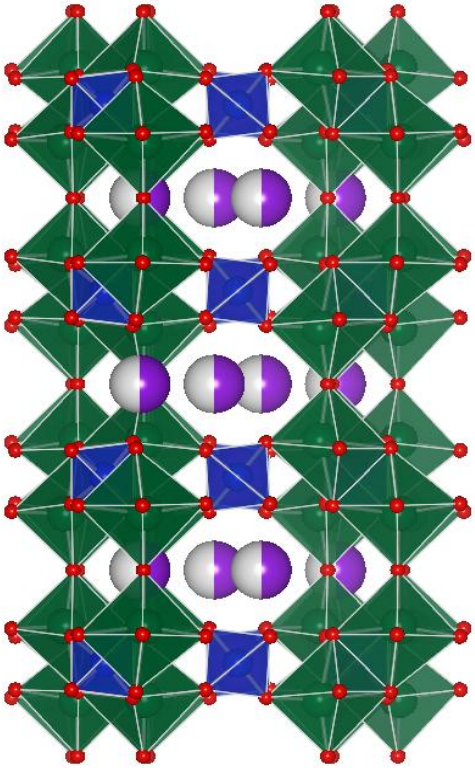
Figure 9: *Cs-TS as seen along the c-axis and a-axis, $P4_2/mcm$ [2]. Cs enters the center of the 8MR, either within the 6MR ring window or just outside it. Interstitial H_2O molecules have been omitted in this view for clarity. Cs = lime green.*

The K^+ ions, being larger than Na^+ yet smaller than Cs^+, do not have an effect on the space group symmetry, and only a minor effect on the unit cell dimensions[26]. In a partial K^+ exchange into H-TS, it was determined by Poojary, et al. (1996) that the center site is preferred and will fill first, in line with the 8MR window much like Cs^+. As more K^+ becomes available the near-framework site fills with partial occupancy to the maximum allowed by space constraints. (See Figure 10) The K^+ is not large enough to force a symmetry change from the center site as Cs^+ had, and K^+ is too large to enter the framework site on the *ac* face and 'pop-up' the structure as Na^+ does. The KH-TS has space symmetry $P4_2/mbc$.

i. View along the c-axis



iii. View along the ab plane expanded



ii. View along the ab plane

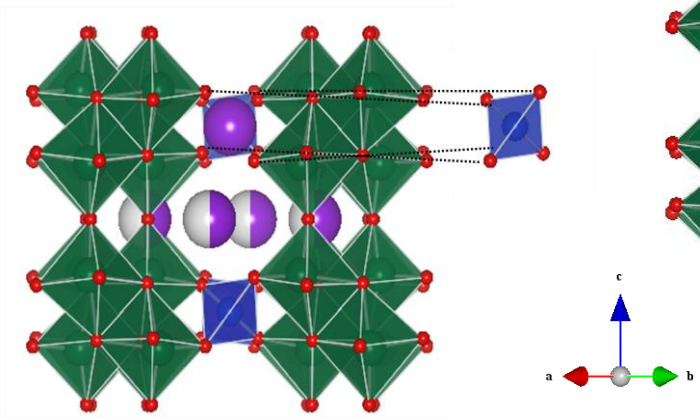


Figure 10*: KH-TS as viewed from the* c *axis and* ab *plane, space group* $P4_2/mbc$, $K_{1.38}H_{0.62}Ti_2O_3SiO_4 \cdot H_2O$. *The first exchanged site is in the center of the 8MR, best seen in i and ii as the solid purple atom. The second exchanged site is near the framework, the purple/white atoms.*

In studies where Sr^{2+} is exchanged into H-TS Tripathi et al. report several symmetry changes as Sr^{2+} occupancy increases[3,31]. The disordered arrangement of water molecules and variable coordination environments are said to have generated both tetragonal and orthorhombic space groups. It is reported that a 25 mol% exchange of Sr^{2+} into the H-TS structure prompts a conformational change to orthorhombic (space group *Cmmm*) while the unit cell dimensions remain similar to those of the protonated phase. The Sr^{2+} is in 10-coordination with five oxygens of the framework and five H_2O molecules, and resides near the framework in the pocket of the 6MR. (Figure 11a) Further loading to 55 mol% Sr^{2+} converts little more than 80% of the TS back into tetragonal (space group $P4_2/mmc$, a subgroup of the Na-TS group $P4_2/mcm$). The position of Sr^{2+} is in two crystallographic sites of the $P4_2/mmc$ structure, the first site having 10-coordination (10-CN) to five framework oxygens and five H_2O molecules. The other site fills to only half occupancy and has either a 7- or 9-CN, five framework oxygens and the rest supplied by H_2O molecules[3,31]. (Figure 11b)

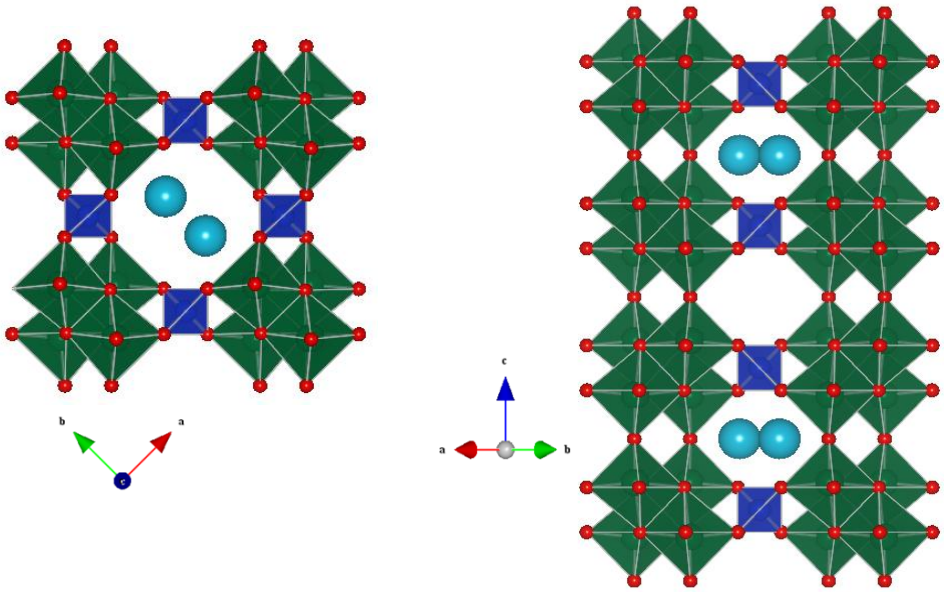


Figure 11a: *SrH-TS as described by Tripathi et al[3]. At a partial occupancy, the space symmetry is Cmmm. Sr enters the near framework site. Interstitial H_2O removed for clarity. Sr = turquoise.*

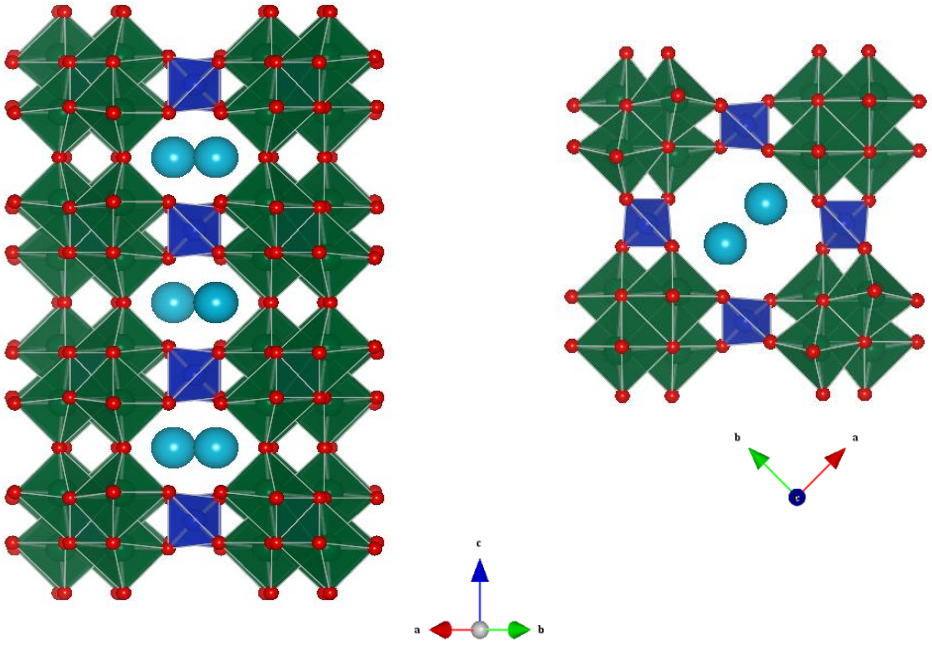


Figure 11b: *SrH-TS as described by Tripathi et al[3]. At higher occupancy the space group changes to $P4_2/mmc$. Sr occupies the near framework site of each void, rather than every other. Interstitial H_2O removed for clarity. Sr = turquoise.*

The niobium doped TS has proved to be challenging to many researchers due to the presence of niobium silicate interference materials generated during synthesis and uncertainties in the Nb^{5+} concentration in the desired material. Initial work has concluded the Na-NbTS structure has a greater affinity for Cs^{+} than the pure Na-TS[27,31].

One distinct advantage of studying the NbTS is that the protonated phase, H-NbTS, retains all the symmetry of the synthesized Na-NbTS, space group $P4_2/mcm$. The structure does not collapse like the H-TS in Figure 7. It is assumed that the larger ionic radius of the Nb^{5+} (in 6-CN is 0.78 Å while Ti^{4+} is 0.745 Å)[32] prevents the structure from twisting into the collapsed phase.

Bearing in mind that the protonated phase is more receptive of larger ions, and that the NbTS will not exhibit an initial symmetry change the author set off to better study the behavior of this novel material as it pertains to Sr^{2+}, and in particular the role of molecular H_2O in the exchange pathways.

Chapter 2

EXPERIMENTAL METHODS

I. Material Synthesis

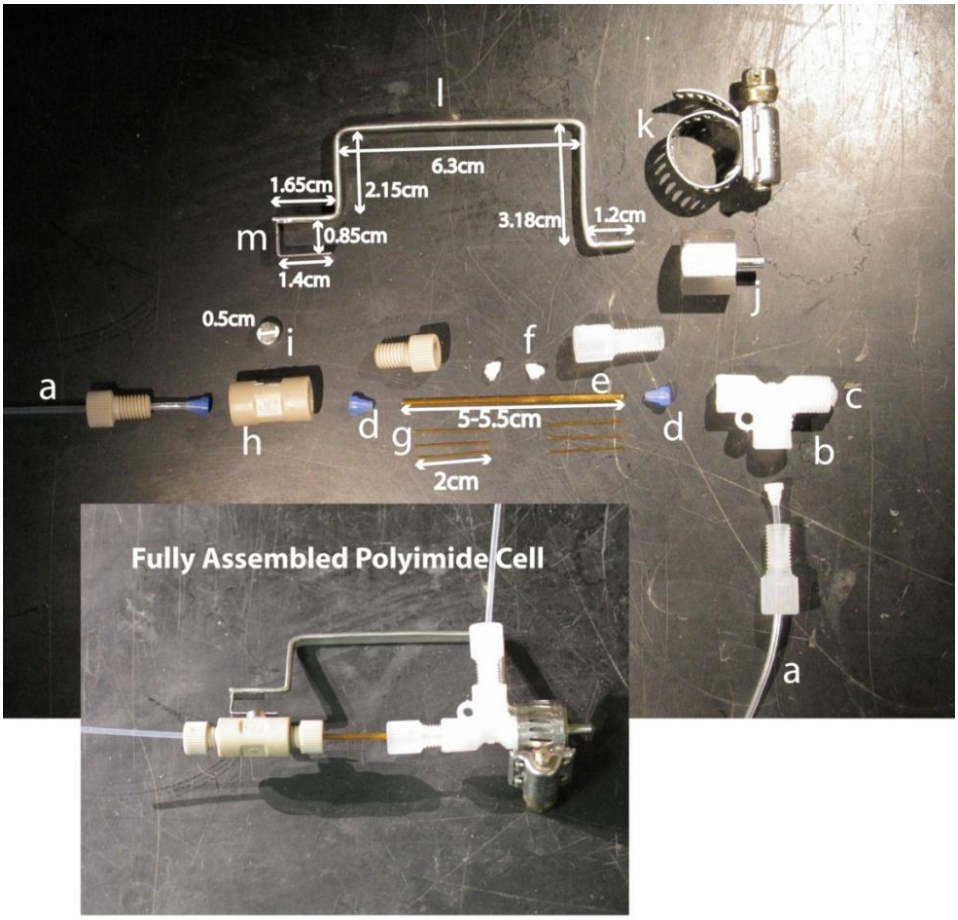
Sodium niobium-titanosilicate (Na-NbTS) has been synthesized by a variety of published processes [3,19,20,26,31]. One of the more successful procedures for producing crystalline NaNbTS has been modeled after Poojary, et al. (1994) and Tripathi et al (2003). The modified synthesis gel includes no less than a Si:Ti/Nb:Na:H_2O mole ratio of 1:1:10:100, Ti and Nb having a 3:1 ratio (25% substitution). The proton exchanged phase is prepared by exhaustively washing the NaNbTS in a 1 M hydrochloric acid solution[26].

II. Time Resolved Ion Exchange

The simultaneous collection of diffraction data as Sr^{2+} ions are exchanged into H-NbTS requires the use of a flow-through experiment cell as seen in Figure 12[14]. The H-NbTS material is lightly packed into the center of a 5 cm length of polyimide tubing (0.0615 in. diameter) and held in place on both sides with glass wool and a 2 cm length spacer of 0.03 in. diameter tubing or three 2 cm lengths of 0.01 in. diameter tubing. Swagelock fittings with ferrules attach the polyimide tube to a goniometer head. The sample cell is plumbed to the ion solution reservoir via plastic tubing.

Three separate experiments were conducted in which H-NbTS was exchanged with100 mL volumes of 0.1 mM, 1.0 mM, and 10.0 mM $SrCl_2$ solutions, respectively.

The ion solution was introduced to the sample at a rate of approximately 1 mL/min in a closed system via a peristaltic pump. The Sr^{2+} ion solutions were prepared at the Brookhaven National Lab facility by the dissolution of strontium chloride crystals in deionized water provided by the facility.



a. Plastic tubing 1/16" O.D.
b. 1/16" flangeless tee union, Tefzel.
c. Sealed end of Tee. Used to fit into 'j'.
d. Flangeless frit-in-ferrule, 0.5mm.
e. Polyimide tube 0.0615" O.D.
f. Glass wool. Used on both sides of powder.
g. Glass wool supports and spacers. Polyimide tubing 0.0215" O.D.
h. 1/16" straight union, PEEK. Magnetic metal adheared to top.
i. REE magnet.
j. Swagelok reducing union, 1/16" to 3/16" male to female.
k. Used to fix the support arm 'l' to 'j'.
l. Support arm. 1/8" stainless steel flexible pipe hammered flat.
m. Magnetic metal. Supports 'i' and 'h'.

Figure 12: *The polyimide environmental cell. Composed of polyimide tubing, glass wool, ferrules, and Swagelok fittings, it can be mounted to a goniometer head and is transferable to multiple instruments. A peristaltic pump is used to drive flow.*

III. Analysis

Powder X-ray Diffraction

The Thermo-Electron Diffractometer, housed at the Materials Characterization Center (now at WKU's Advanced Materials Institute), was used for the *ex situ* and preliminary studies. The X-ray tube contains a copper target ($K\alpha_1$ = 1.54 Å) and operates at 40 kV and 40 mA. Data was collected at room temperature between 8° and 65° 2 θ, with a step size of 0.02°, and a count time of 10 sec/step.

In situ studies were conducted at the National Synchrotron Light Source (NSLS), Brookhaven National Laboratory, New York. The X7B beamline at NSLS has a source sufficient enough to enable the user to collect time-resolved *in situ* data. The beamline yields a flux of more than $1x10^{11}$ photons/sec, operating at approximately 38.9 keV, producing X-rays with a wavelength of 0.3184(3) Å.

A MAR345 imaging plate detector with a built in scanner is installed on the beamline[33] and was positioned 375 mm from the sample holder during these experiments. Data was accumulated in 60 second exposures on the imaging plate. The plate was scanned, the data exported to the consol and the imaging plate erased. Data cannot be collected for approximately 60 seconds while the imaging plate is scanned and erased. The beam center, detector distance, and intensity are calibrated with a lanthanum hexaboride standard. The goniometer head fitted with the polyimide exchange cell (Figure 12) is mounted to the stage of the X7B beamline, and plumbing lines attached once the sample is centered in the path of the beam. Data were collected continuously during each of these experiments, lasting approximately ten hours each.

The imaging plate data were integrated by the software FIT2D[34] into a universal ASCII format, 2θ vs. intensity, by entering the beam calibration file and the beam line parameters. Data could then be converted again with the program ConvX[35] into .gsas file format or other extensions. Rietveld structure refinements were completed with GSAS-EXPGUI[36,37] and FullProf Suite[38] programs.

Chapter 3

RESULTS and DISCUSSION

I. X-Ray Diffraction and Phase Transitions

Each experiment (where Exp A = 0.1 mM Sr^{2+} solution, Exp B = 1.0 mM, and Exp C = 10.0 mM) was allowed to run approximately ten hours, recirculating the respective Sr^{2+} ion solution in hopes of reaching chemical equilibrium and uniform exchange. Diffraction data were collected throughout the experiment in approximately two minute increments. Few dramatic changes can be seen in the diffraction pattern (Figure 13) aside from the gradual decline in general beam intensity (the beam decays as a natural function of the synchrotron light source design and is regenerated every 12 hours). It is only upon careful inspection that we observe first, the general intensity of the largest peak (100) decreases quite dramatically at the introduction of the ion exchange solution. Second, the generation of a new peak is observed in the diffraction pattern at approximately 1.4° 2θ.

This new peak identifies the 001 reflection, a reflection that is not allowed by the $P4_2$/mcm space group (the space group of the H-NbTS, our starting material). As the peak exists in the diffraction pattern, this indicates a structural transformation has occurred. The last useable frame of Exp C (10.0 mM Sr^{2+} ion solution) records the greatest exposure time with Sr, and ideally the greatest exchange or greatest quantity of structurally transformed material has been reached. This frame will show the most exchanged phase and contain the model and symmetry information of the final structure. This last pattern was indexed utilizing powder diffraction indexing software, Poudrix[39],

to determine the most probable space group symmetry of the new structure. The most reasonable space group is P-42m, a supergroup of $P4_2/mcm$ (H-NbTS) and allows for all the reflections seen in the diffraction pattern to be indexed.

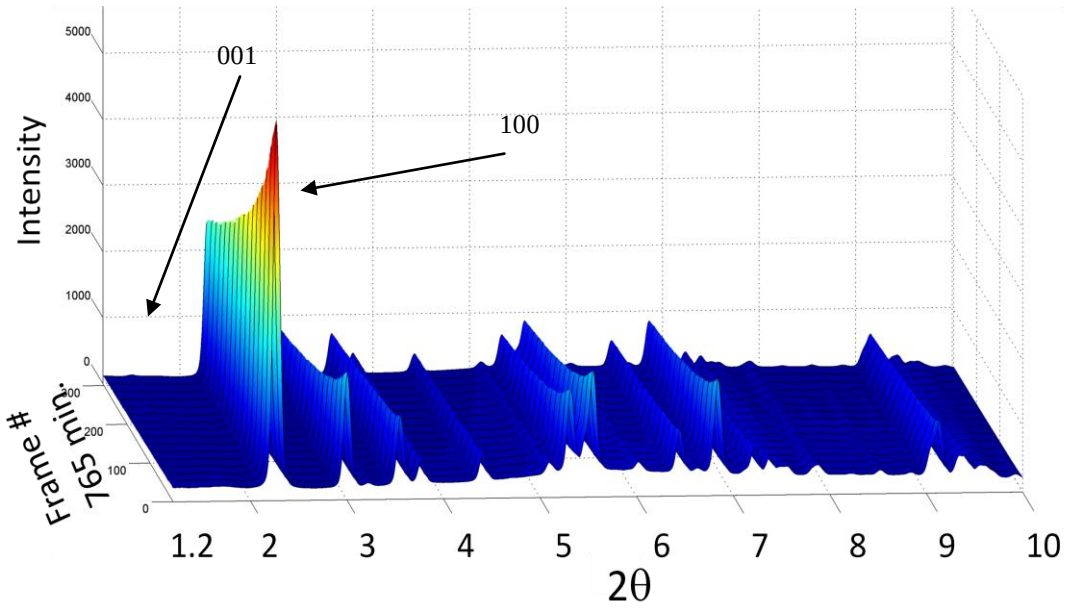
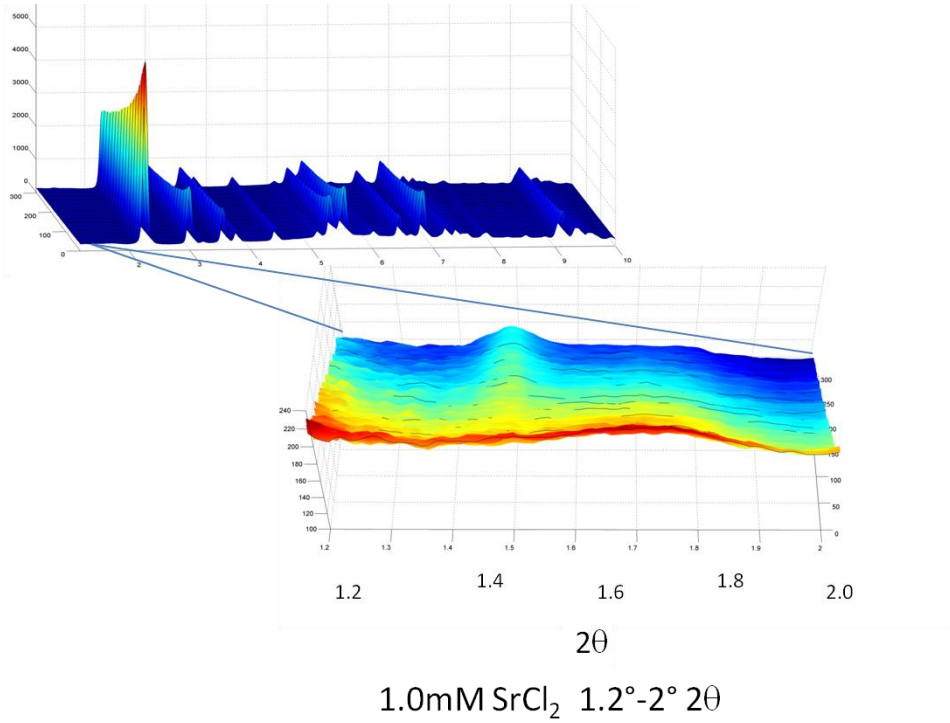


Figure 13: *A time-resolved, 3-D, compilation of diffraction patterns gathered over the course of exchange of 1.0 mM $SrCl_2$ solution with HNbTS, Exp B.*

Monitoring the estimated peak evolution of the 001 peak with ITTFA (iterative target transform factor analysis) statistically confirms its presence, relative to background, as Sr sequestration proceeds. This can be viewed in Figures 14a and 14b. Exchange in Exp B, the 1.0 mM Sr^{2+} ion solution, shows that the peak appears approximately 60 minutes after the introduction of the solution. In Exp C, the more concentrated solution, the 001 peak is seen after 16 minutes.



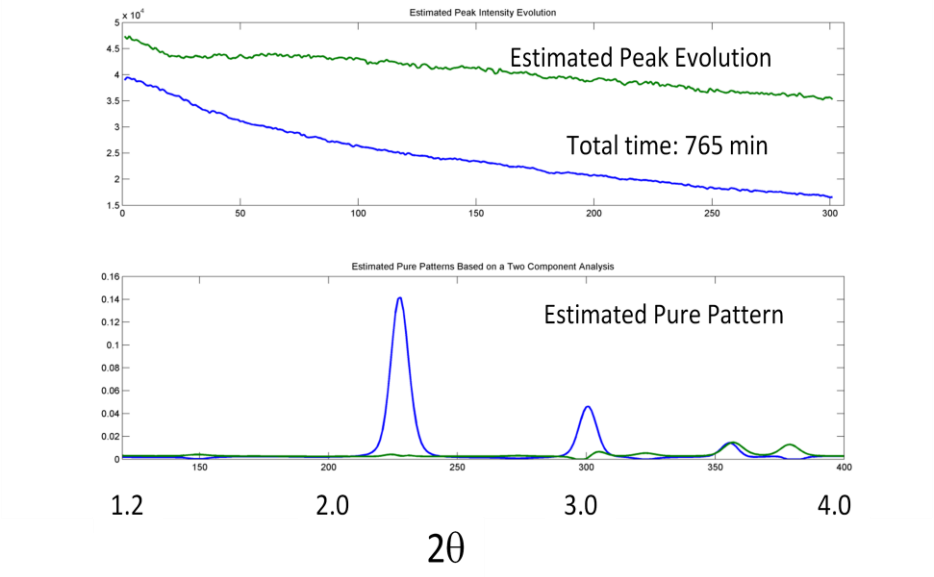


Figure 14a: *Estimated peak evolution, obtained by ITTFA, of the 001 peak in the exchange of 1.0mM $SrCl_2$ solution with H-NbTS. The 001 peak can be seen after approximately 60-minutes of exchange.*

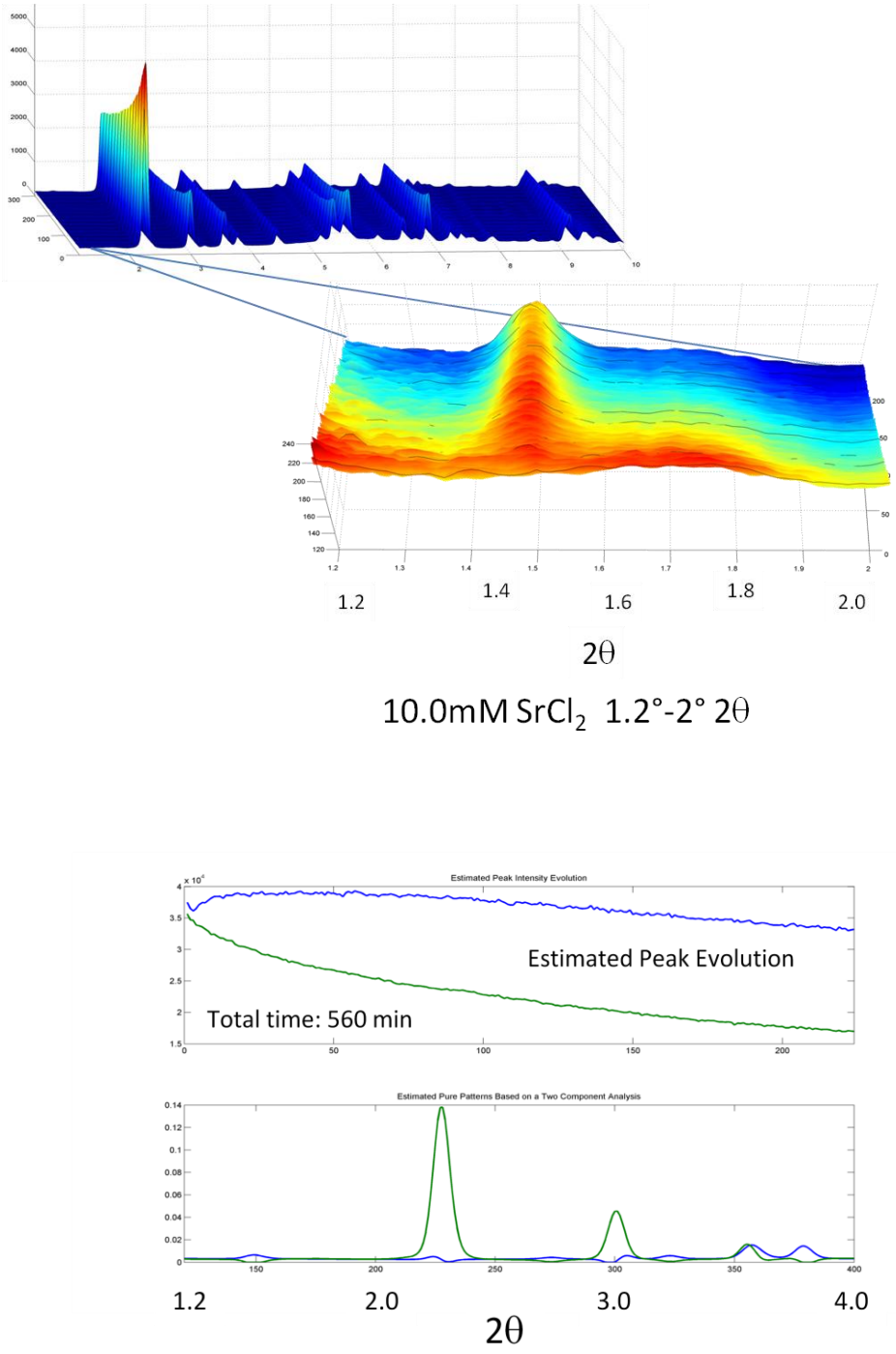


Figure 14b: *Estimated peak evolution, obtained by ITTFA, of the 001 peak in the exchange of 10.0mM $SrCl_2$ solution with H-NbTS. The 001 peak can be observed after 16 minutes of exchange.*

Confirming the presence of the new peak has led to obtaining a different symmetry for the new phase, P-42m. In comparing the two symmetries, the exchanged phase exhibits lower symmetry generated by a loss of translation along the c-axis, i.e.: the 4_2 screw is reduced to a -4.

II. Rietveld Structure Refinements

The time-resolved X-ray diffraction data were refined using the EXP-GUI interface for GSAS[36,37]. The structure for the material before exchange, H-NbTS, was modeled after Tripathi et al. in the $P4_2/mcm$ symmetry[31]. Diffraction data was first collected on the H-NbTS material as only deionized water was flushed through the system. Having water in these initial refinements better simulates experimental conditions than data from dry H-NbTS material. The scattering effects of the water flowing external to the crystals needed to be accounted for in the background signals. The collected data were refined to verify the material composition and structural model for the $P4_2/mcm$ phase. The diffraction pattern for H-NbTS can be seen in Figure 15.

The framework metal sites did not move from the transformed model when refined with medium restraints, and were retained. The electron density of the framework oxygens could not be adequately modeled apart from the large metal ions, resulting in chemically invalid structural positions. Framework oxygen sites were retained from the transformed model. The Ti/Nb occupancy ratio was refined from 0.75/0.25 to 0.70/0.30. In all examinations data below 1.2° and above 15.0° 2θ (0.61 Å) were excluded from refinements as data outside these ranges exhibited the greatest interference of scattering effects. The model of H-NbTS is shown in Figure 16.

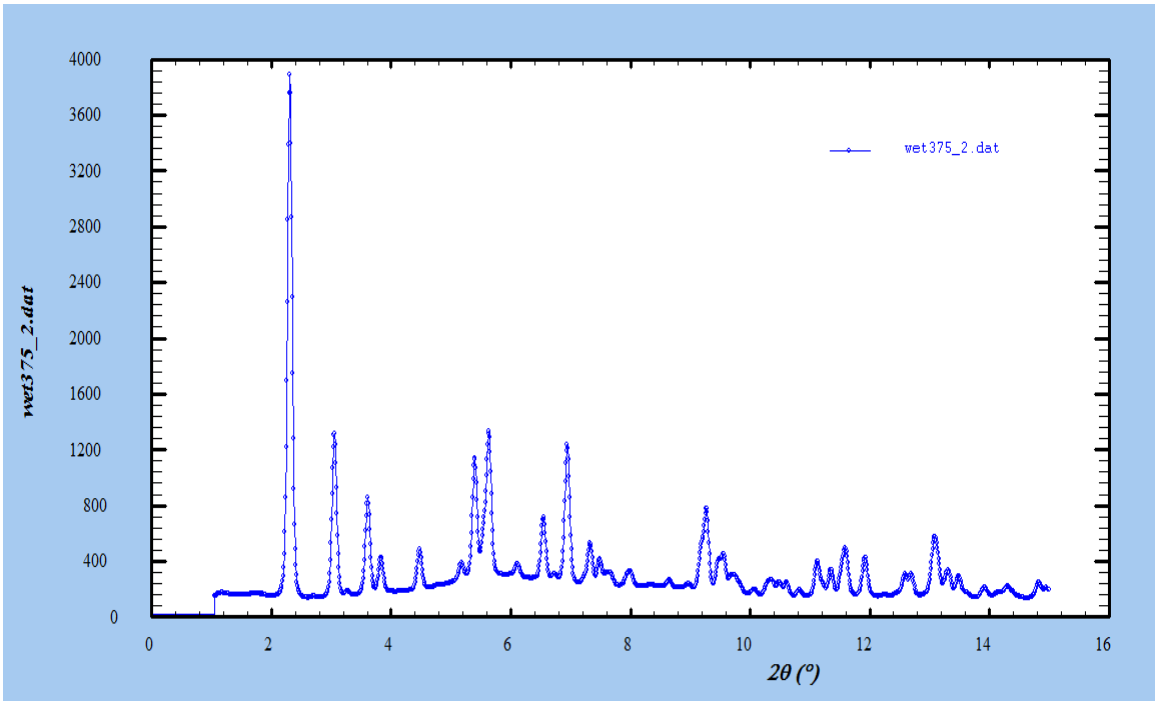


Figure 15: *Diffraction pattern of H-NbTS, collected at the NSLS with deionized water circulating through the exchange cell. Image captured in FullProf Suite WinPlotR*[38].

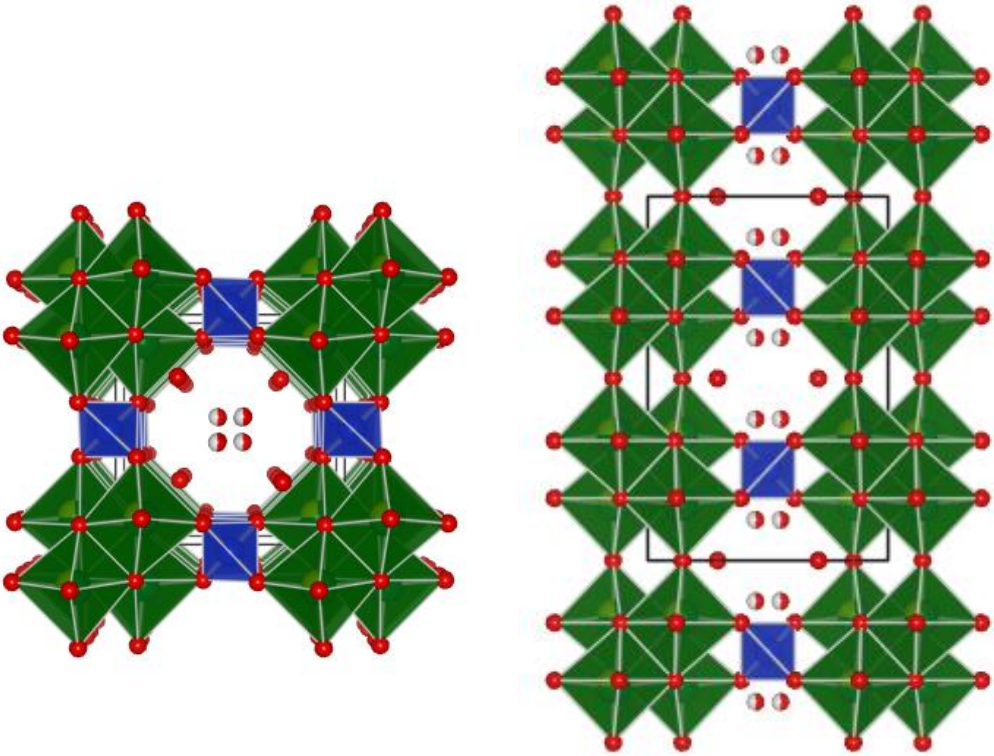


Figure 16: *H-NbTS as seen along the c-axis and the a-axis. Note the position of the interstitial H_2O molecules, the free red atoms and red/white atoms.*

Examination of the experimental data began with the highest concentration and greatest exchange, Exp C. A new structural model was obtained by transforming the refined $P4_2/mcm$ structure parameters into the P-42m space group. The transformation was completed with crystallographic software, Powdrix[40] Each diffraction pattern examined was modeled via Le Bail refinements[41] to obtain unit cell and profile parameters. The profiles were modeled using a Thompson-Cox-Hastings pseudo-Voigt function[42] where only U, V, and W full width half maximum parameters, the instrument zero, and X and Y shape parameters were refined. The calculated profile could be refined to below a X^2 value of 1.00. The same Gaussian peak parameters and the instrument zero were utilized in all subsequent refinements, while the Lorentzian function parameters are refined for each frame. The unit cell parameters, *a* and *c*, were initially refined each time but were later fixed when it became apparent the unit cell dimensions only changed within the range of error from the transformed model. Each diffraction pattern did have a unique background profile which had to be fit manually by selecting a series of points and then refining them with maximum restraints in place.

Structural models were refined using Rietveld methods[1] to obtain occupancies and positions of the extra framework H_2O molecules and Sr^{2+} ions. The framework metal ions and oxygen positions were not refined from the transformed results because the unit cell parameters did not change outside the range of error. Fourier difference maps were generated from the GSAS program to visually assess electron density differences between the observed structure model and the computed model. This is done by overlying the DELF map with the current 3D structure model in VESTA[43]. Peaks found

in the DELF maps could be interjected into the structure model to better refine positions and occupancies.

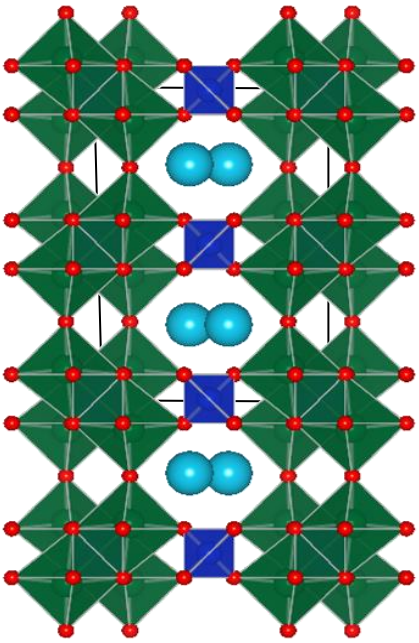
Table 3: Refinement parameters of the H and Sr exchanged niobium-titanosilicate

	H-NbTS	**SrH-NbTS**
Formula	$H_{1.7}Nb_{0.3}Ti_{1.7}SiO_7 \cdot 1.9H_2O$	$Sr_{0.21}H_{1.28}Nb_{0.3}Ti_{1.7}SiO_7 \cdot 2H_2O$
fw	1162.8	1253.6
Space Group	*$P4_2/mcm$*	*P-42m*
***a*, Å**	7.848(2)	7.961(8)
***c*, Å**	11.889(2)	12.039(2)
Volume, Å^3	732.6	763.1
$d_{cal'd}$, g/cm^3	2.636	2.728
Fitted R_{wp}	0.1223	0.1053
Fitted R_p	0.0962	0.0773

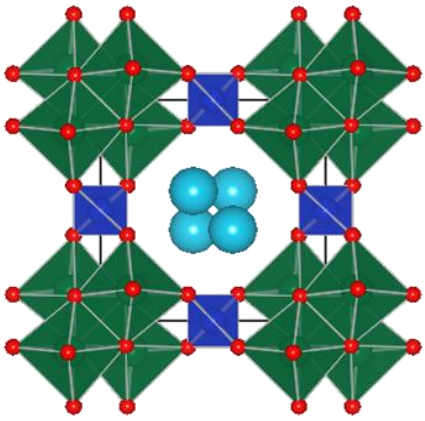
Strontium position and Symmetry Change

Refining the final usable frame of Exp C, Sr was found to reside near the apical oxygen of the Nb/Ti octahedron (O5), bonding to it and the four closest framework oxygens. This is analogous to the near framework site summarized by Clearfield[27]. Here Sr can reach a total coordination of nine by bonding with those five framework oxygens and four H_2O molecules, one above (Ow2), one below (Ow3), and two off the side (Ow1). Figure 17 offers visual aid in the placement of Sr and the interstitial H_2O molecules.

i. View along *a*-axis



ii. View along *c*-axis



iii. View of Sr and H_2O

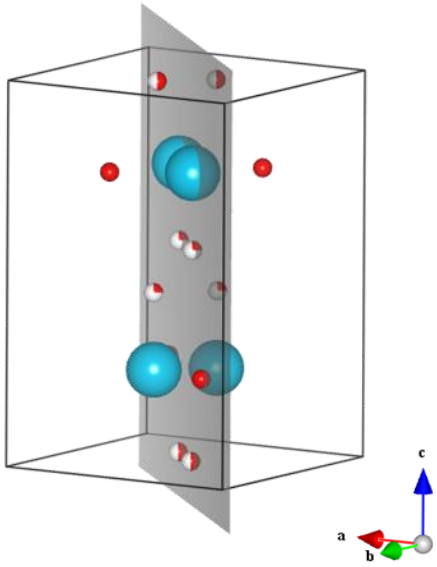


Figure 17: *Models of SrH-NbTS as viewed along the* a*-axis (i) and* c*-axis (ii), and a simplified model of the Sr and H_2O positions (iii). Sr = turquoise, H_2O = red and red/white, unit cell = black lines, 110 reflection = gray plane.*

When Sr occupies its position in the channel, H_2O molecules migrate to stabilize the coordination of the larger, more covalent ion (more covalent than a proton or Na^+). It is this relocation of water that warrants the loss of symmetry and subsequent change in space group (ie: $P4_2/mcm$ to P-42m), not the position of Sr. The unit cell shifts one quarter of its length along *c*, placing the plane of silica tetrahedrons at the ends and center of the unit cell rather than at one and three quarters as in the H-NbTS structure. (Figure 18)

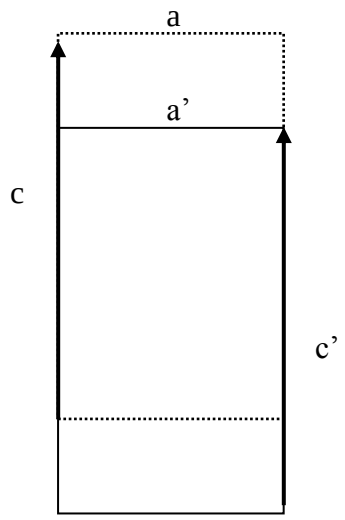


Figure 18: *Relationship between the unit cell dimensions of the space groups $P4_2/mcm$ and P-42m.*

The inter-atomic distances between Sr and the oxygens of the framework are longer than those to H_2O. It is the strong repulsion of the cationic charges of Nb/Ti and Sr that make this so, lessening the bond valence of the framework oxygens. The oxygens of the H_2O molecules are more closely bound to supply the necessary charge balance. Bond valence sum calculations were completed[44] to verify the viability of the modeled

Sr-O bonds. Calculations support the conclusion that the four water O-Sr bonds contribute more to the valence sum than do the five framework O-Sr bonds.

Table 4: Strontium-oxygen interatomic distances (Å) in SrH-NbTS.

Sr-O2	3.046(5) x 2	Sr-Ow1	2.608(2) x 2
Sr-O5	3.027(1)	Sr-Ow3	3.121(7)
Sr-O1	3.198(5) x 2	Sr-Ow2	3.048(7)

The H_2O molecule modeled as Ow2 in H-NbTS will not occupy the same position in the new unit cell, within the center, as it cannot be translated along *c* with Sr sequestered. The Ow2 site is split in the new unit cell, labeled as Ow2 and Ow3. Figure 19 shows the Sr-O bonding geometries as modeled from the refinements.

Refinements with the P-42m space group are stable, reaching a convergence X^2 value below 3.0. Attempts to model both the beginning phase (H-NbTS) and end phase (SrH-NbTS) simultaneously were inconclusive, as there is significant peak overlap.

The procedures utilized to examine Exp C were used for the mid concentration, Exp B, 1.0 mM Sr^{2+} solution, as well. The time-resolved compilation of diffraction data by ITTFA showed the presence of the 001 reflection after approximately 60 minutes of ion exchange. This means a significant quantity of the P-42m phase is now present and Sr^{2+} has been sequestered.

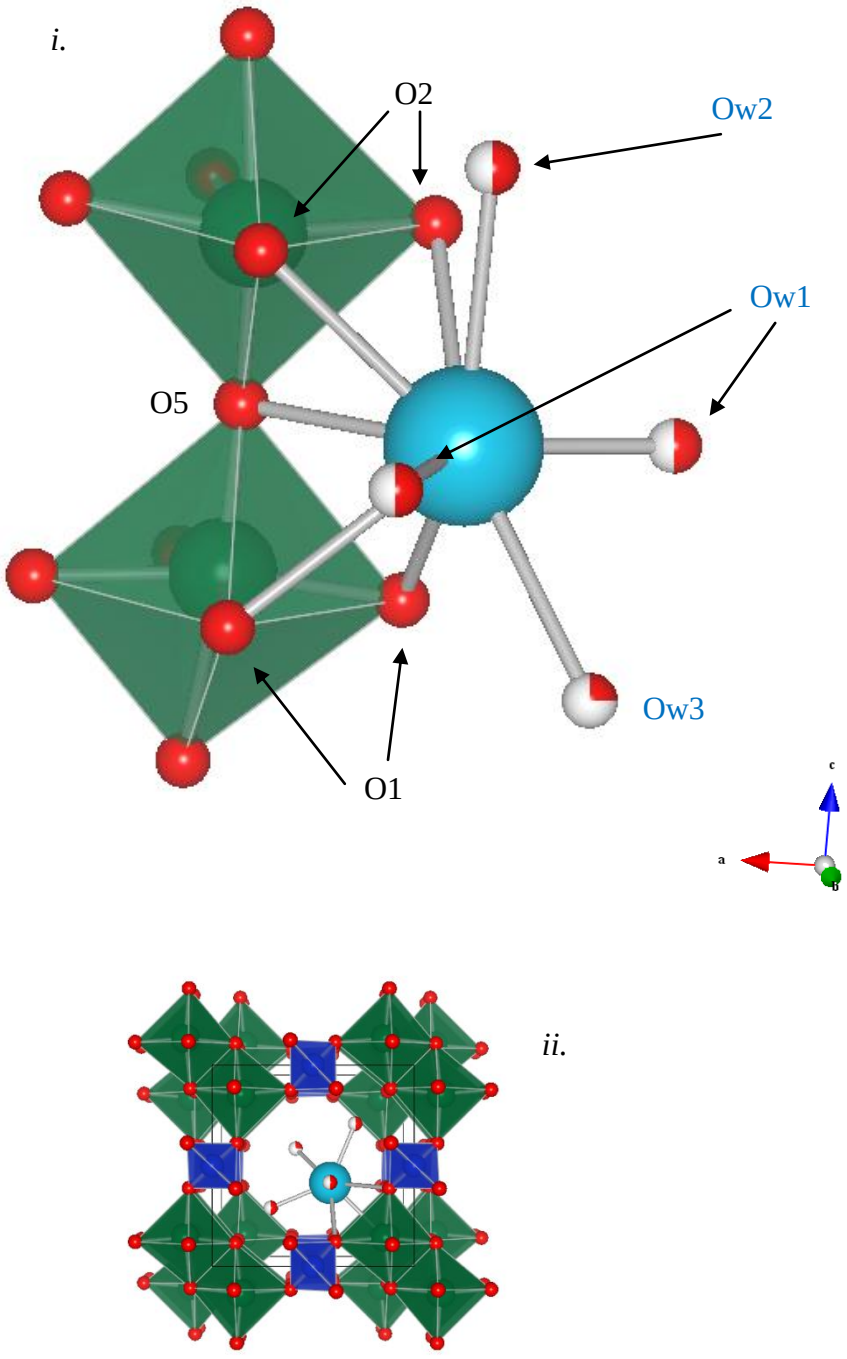


Figure 19: *Bond geometry for SrH-NbTS, as modeled from Rietveld structure refinements. Sr forms bonds with five framework oxygens and four interstitial H_2O molecules, labeled in (i). A view along the c-axis is displayed in (ii).*

Strontium Occupancy and Mechanism

The fractional occupancy of Sr^{2+} in its refined location was also determined during Rietveld structure refinements. The maximum occupancy attained during the experiments was 21.1(4) %, as refined from the last frame of Exp C. By strategically selecting frames throughout each experiment, the author had hoped to observe any critical shifts in occupancy or ion position, as well as phase composition. Sr occupancy could be reasonably modeled. The first frames of Exp. A (0.1 mM Sr^{2+} solution) were refined to a Sr^{2+} ion occupancy of around 5.0(5) %. Strontium is immediately taken into the material and absorption increases steadily throughout this experiment to 12.2(4) % occupancy.

Experiment B (1.0 mM Sr^{2+} solution) begins as Exp. A did, with an initial uptake of approximately 5.1(2) %, but reaches 12.4(1) % soon before the 60 minute mark, where the first observance of the 001 reflection is found. In the support of this pattern, in Exp. C (10.0 mM Sr^{2+} solution) Sr^{2+} ion occupancy reaches 12-15% just before the 001 reflection is observed; 16 minutes into the experiment.

Based on the working model that the sequestration of Sr^{2+} into H-NbTS facilitates the relocation of H_2O molecules, namely Ow3, forcing a new phase symmetry, it is concluded that the P-42m space group (i.e.: our exchanged phase) is the best symmetry description for every exchanged unit cell. Prior to exchange reaching approximately 12-15% Sr occupancy, the 001 reflection is absent, and the space group has not changed.

The process seems kinetically driven, in that Ow2 requires 12-15% of Sr loading before splitting into the Ow3 site. Mechanistically, Sr enters the 8MR channel

surrounded by a hydrosphere. The preferred bonding orientation is to position Sr near the framework, bonding to five framework oxygens. The remaining bond valence is provided by four H_2O molecules. As Sr occupancy is increased, the position and orientation of water within the channel migrates to alleviate space constraints and ionic repulsive forces. At an occupancy of 12-15% the Ow3 position is such to generate a loss in symmetry to the P-42m space group. A plot of Sr occupancy as the exchange progresses is displayed in Figure 20.

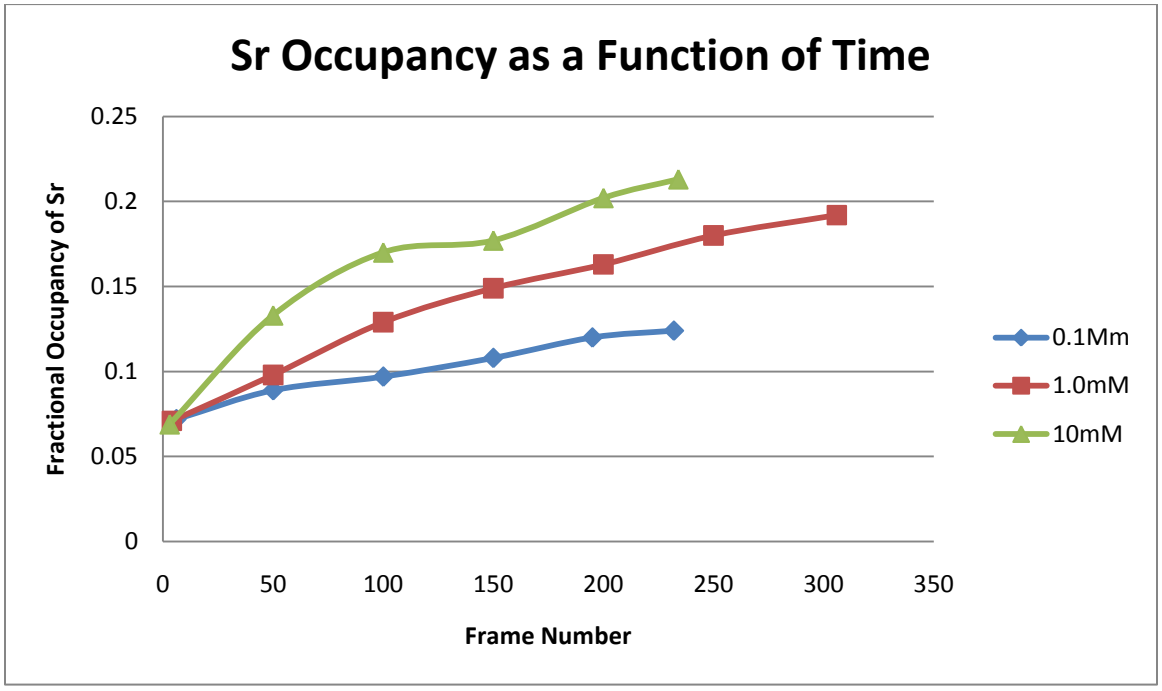


Figure 20: *Plot of Sr occupancy vs. frame number. The frame number can be interpreted as time, as a frame was collected approximately every two minutes. 300 frames is equivalent to approximately 10 hours of exchange.*

Chapter 4

CONCLUSIONS

Time resolved powder diffraction is an excellent way to study the exchange of ions into porous materials. High resolution diffraction patterns collected at the NSLS allowed for the determination of the correct space group and atomic positions of ions in the SrH-NbTS. Sr was successfully exchanged into the structure to 21% occupancy, and is bound in the structure by five framework oxygens and four oxygens of H_2O molecules for a total coordination of nine. The exchanged material has a space group symmetry of P-42m.

Previous studies reported the SrH-NbTS as having a similar Sr^{2+} ion position within the channel but being of the $P4_2$/mcm space group[31]. The lack of *in situ* data may be why the SrH-NbTS was misclassified in the previous studies. The observance of the 001 reflection is imperative in modeling the correct symmetry group, seen only with low angle resolution and time resolved data.

Neutron diffraction studies will need to be completed to accurately determine hydrogen positions, allowing for the orientation of water and free protons to be modeled. It will also better elucidate the occupancy of Sr and H as ion exchange proceeds. The observed speed with which Sr^{2+} is sequestered has made modeling a stepwise mechanism extremely difficult. It is hoped neutron data will help in this endeavor as well.

Other methods of determining the quantity of interstitial water should also be explored, such as thermal gravimetric analysis (TGA), or X-ray diffraction experiments utilizing environmental sample cells to control water vapor pressures and temperatures[45].

Current and future work possibilities include studying the sequestration mechanisms of Ca and Mg. These divalent ions, being smaller than Sr, can offer valuable insight into the pathway characteristics of porous materials and ion selectivity. Another interesting study would be the diffusion effects of ions through a larger crystal.

APPENDIX A

Atomic Positions of H-NbTS

Atom	*x*	*y*	*z*	occupancy	Uiso*
Si	0.0000	0.5000	0.2500	1.0	0.01267
Ti	0.1392	0.1392	0.1541	0.70	0.01267
Nb	0.1392	0.1392	0.1541	0.30	0.01267
O1	0.1195	0.3876	0.1710	1.0	0.03800
O2	0.1126	0.1120	0.3289	1.0	0.03800
O4	0.1439	0.1439	0.0000	1.0	0.03800
Ow1	0.2901	0.2901	0.5000	1.0	0.07599
Ow2	0.4479	0.4479	0.1117	0.4886	0.07599

* Isotropic displacement parameters were converted from published values by Tripathi et al., 2003[3].

** Occupancy of Ow2 and the Ti/Nb sites were the only parameters refined when establishing the H-NbTS phase prior to exchange. The atomic coordinates are taken from Tripathi et al., 2003[31].

APPENDIX B

Atomic Positions of SrH-NbTS

Atom	*x*	*y*	*z*	occupancy	Uiso*
Si1	0.5000	0.000	0.0000	1.0	0.01267
Si2	0.5000	0.000	0.5000	1.0	0.01267
Ti1	0.1392	0.1392	0.09590	0.70	0.01267
Ti2	0.1392	0.1392	0.40410	0.70	0.01267
Nb1	0.1392	0.1392	0.09590	0.30	0.01267
Nb2	0.1392	0.1392	0.40410	0.30	0.01267
O1	0.1195	0.3876	0.4210	1.0	0.03800
O2	0.6124	0.119	0.9211	1.0	0.03800
O3	0.1120	0.1120	0.9211	1.0	0.03800
O4	0.1120	0.1120	0.5789	1.0	0.03800
O5	0.1439	0.1439	0.2500	1.0	0.03800
Ow1	0.285(5)	0.285(5)	0.755(1)	1.0	0.07599
Ow2	0.417(4)	0.582(5)	0.012(8)	0.50	0.07599
Ow3	0.41(0)	0.58(9)	0.56(0)	0.25	0.07599
Sr1	0.412550	0.412550	0.240378	0.211(4)	0.07599

* Isotropic displacement parameters were converted from published values by Tripathi et al., 2003[3].

APPENDIX C

Bond Valence Sum Calculations

Program VaList version Win95,98,NT
Bond Valence calulation program v.1.0
Release : January 1999

Andrew S. Wills
copyright: Commissariat à l'Energie Atomique, France
Bond valences provided by I.D. Brown
***** Version 1.0 for Windows *****

Please reference the use of this program as:
A.S. Wills and I.D. Brown, VaList, CEA, France (1999). Program available from author at willsas@netscape.net.

****

Bond valence for bond ij is defined by: s(ij)=(exp[R0(ij)-R(ij))/B(ij)])
Sum of bond valances = Sigma s(ij), summed over all i,j

****

References to the bond valences:

a Brown and Altermatt, 1985, Acta Cryst. B41, 244-247 (empirical)
b Brese and O'Keeffe, 1991, Acta Cryst. B47, 192-197 (extrapolated)
c IDB Private communication
d IDB Private communication
e IDB Private communication
f Brown, Gillespie, Morgan, Tun and Ummat 1984, Inorg. Chem. 23, 4506-4508
* Unchecked

****

FileName: C:\Documents and Settings\wkuuser\Desktop\SR03_324b.cif
Structural chemical formula: Structural chemical formula: ?
Chemical formula sum: Chemical formula sum: Nb0.60 O9.00 Si Sr0.21 Ti1.40

****

Selected bond valence sums:

Atom no.	Oxidn. state assumed	Most consistent oxidn. state	Bond Valence Sum	% Deviation from assumed oxidn. state
TI1	(4)	*	3.699	8
NB1	(5)	*	4.794	4
TI2	(4)	*	3.699	8
NB2	(5)	*	4.794	4
SI1	(4)	*	4.12	3
SI2	(4)	*	4.12	3
SR1	(2)	*	2.185	9

Bond valence parameters:

	bond length	oxidn. state assumed	R0	B	s(ij)	parameter reference
TI1_O2	1.995	TI(4)	1.815	0.37	.615	a
TI1_O2	1.995	TI(4)	1.815	0.37	.615	a
TI1_O3	2.127	TI(4)	1.815	0.37	.43	a
TI1_O3	2.022	TI(4)	1.815	0.37	.572	a
TI1_O3	2.022	TI(4)	1.815	0.37	.572	a
TI1_O5	1.856	TI(4)	1.815	0.37	.895	a
NB1_O2	1.995	NB(5)	1.911	0.37	.797	a
NB1_O2	1.995	NB(5)	1.911	0.37	.797	a
NB1_O3	2.127	NB(5)	1.911	0.37	.558	a
NB1_O3	2.022	NB(5)	1.911	0.37	.741	a
NB1_O3	2.022	NB(5)	1.911	0.37	.741	a
NB1_O5	1.856	NB(5)	1.911	0.37	1.16	a
TI2_O1	1.995	TI(4)	1.815	0.37	.615	a
TI2_O1	1.995	TI(4)	1.815	0.37	.615	a
TI2_O4	2.127	TI(4)	1.815	0.37	.43	a
TI2_O4	2.022	TI(4)	1.815	0.37	.572	a
TI2_O4	2.022	TI(4)	1.815	0.37	.572	a
TI2_O5	1.856	TI(4)	1.815	0.37	.895	a
NB2_O1	1.995	NB(5)	1.911	0.37	.797	a
NB2_O1	1.995	NB(5)	1.911	0.37	.797	a
NB2_O4	2.127	NB(5)	1.911	0.37	.558	a
NB2_O4	2.022	NB(5)	1.911	0.37	.741	a
NB2_O4	2.022	NB(5)	1.911	0.37	.741	a
NB2_O5	1.856	NB(5)	1.911	0.37	1.16	a
SI1_O2	1.613	SI(4)	1.624	0.37	1.03	b

SI1_O2	1.613	SI(4)	1.624	0.37	1.03	b
SI1_O2	1.613	SI(4)	1.624	0.37	1.03	b
SI1_O2	1.613	SI(4)	1.624	0.37	1.03	b
SI2_O1	1.613	SI(4)	1.624	0.37	1.03	b
SI2_O1	1.613	SI(4)	1.624	0.37	1.03	b
SI2_O1	1.613	SI(4)	1.624	0.37	1.03	b
SI2_O1	1.613	SI(4)	1.624	0.37	1.03	b
SR1_O1	3.199	SR(2)	2.118	0.37	.054	a
SR1_O1	3.199	SR(2)	2.118	0.37	.054	a
SR1_O2	3.047	SR(2)	2.118	0.37	.081	a
SR1_O2	3.047	SR(2)	2.118	0.37	.081	a
SR1_O5	3.027	SR(2)	2.118	0.37	.086	a
SR1_O11	2.608	SR(2)	2.118	0.37	.266	a
SR1_O11	2.608	SR(2)	2.118	0.37	.266	a
SR1_O12	3.056	SR(2)	2.118	0.37	.079	a
SR1_O12	3.056	SR(2)	2.118	0.37	.079	a
SR1_O12	3.049	SR(2)	2.118	0.37	.081	a
SR1_O13	3.122	SR(2)	2.118	0.37	.066	a
SR1_O13	2.403	SR(2)	2.118	0.37	.463	a
SR1_O13	3.122	SR(2)	2.118	0.37	.066	a
SR1_O13	2.403	SR(2)	2.118	0.37	.463	a

****

WARNING: Users MUST check the validity of GII calculation. See HELP.RTF for details.
Global Instability Index: .22

****

VaList calculations completed

REFERENCES

(1) Rietveld, H. M. *J of Applied Cystallography* **1969**, *2*, 65-71.

(2) Celestian, A. J., Parise, J.B., Smith, R., Toby, B.H., Clearfield, A. *Inorg. Chem.* **2007**, *46*, 1081-1089.

(3) Tripathi, A., Medvedev, D., Clearfield, A. *J of Solid State Chem,* **2005**, *178*, 253-261.

(4) In *International Conference on Molecular Sieve Zeolites*; Gould, R. F., Ed.; American Chemical Society: Worcester, MA, 1970; Vol. 101, p 525.

(5) Colella, C.; Gualtieri, A. F. *Microporous and Mesoporous Materials* **2007**, *105*, 213-221.

(6) Cronstedt, A. F. In *Akad. Handl.* Stockholm, 1756; Vol. 180.

(7) Breck, D. W. *Zeolite Molecular Sieves*; John Wiley and Sons: New York, 1974.

(8) Tsitsishvili, G. V.; Andronikashvili, T. G.; Kirov, G. N.; Filizova, L. D. *Natural Zeolites*; Ellis Horwood Limited: Chichester, England, 1992.

(9) McBain, J. W. *The Sorption of Gases and Vapors by Solids*; Rutledge and Sons: London, 1932.

(10) Chukanov, N. V.; Pekov, I. V. In *Reviews in Mineralogy and Geochemistry*; MIneralogical Society of America: 2005; Vol. 57, p 105-143.

(11) Zagorodni, A. A. *Ion Exchange Materials: Properties and Applications*; Elsevier: Amsterdam, 2007.

(12) Helfferich, F. G.; McGraw Hill: New York, 1962.

(13) Harland, C. E. *Ion Exchange: theory and practice*; Royal Society of Chemistry: London, 1994.

(14) Celestian, A. J.; Kubicki, J. D.; Parise, J. B.; Clearfield, A.; Hanson, J. *J. Am. Chem. Soc.* **2008**, *130*, 11689-11694.

(15) Celestian, A. J., Medvedev, D.G., Tripathi, A., Parise, J.B., Clearfield, A. *Nuclear Instru. and Methods* **2005**, *238*, 61-69.

(16) Barrer, R. M. *Zeolite and Clay Minerals as Sorbents and Molecular Sieves*; Academic Press: London, 1978.

(17) In *International Conference on Molecular Sieve Zeolites*; Gould, R. F., Ed.; American Chemical Society: Worcester, MA, 1970; Vol. 102, p 459.

(18) Anthony, R. G.; Philip, C. V.; Dosch, R. G. *Waste Management* **1993**, *13*, 503-512.

(19) Pertierra, P., Salvado, M., Garcia-Granda, S. *Inorg. Chem.* **1999**, *38*, 2563-2566.

(20) Poojary, D. M., Cahill, R.A., Clearfield, A. *Chem. Mater.* **1994**, *6*, 2364-2368.

(21) *Science and Technology for Disposal of Radioactive Tank Wastes*; Schulz, W., Lombardo, N., Ed.; Plenum Press: New York, 1998.

(22) Ibarra, I. A.; Lima, E.; Loera, S.; Bosch, P.; Bulbulian, S.; Lara, V. *The Journal of Physical Chemistry B* **2006**, *110*, 21086-21091.

(23) Dyer, A.; Abou-Jamous, J. *Journal of Radioanalytical and Nuclear Chemistry* **1997**, *224*, 59-66.

(24) Dyer, A.; Las, T.; Zubair, M. *Journal of Radioanalytical and Nuclear Chemistry* **2000**, *243*, 839-841.

(25) Sokolova, E. V.; Rastsvetaeva, R. K.; Andrianov, V. I.; Engorov-Tismenko, Y. K.; Men'Shikov, Y. P. *Dokl. Akad Nauk SSSR* **1989**, *307*, 114.

(26) Poojary, D. M., Borton, A.I., Borton, L.N., Clearfield, A. *Inorg. Chem.* **1996**, *35*, 6131-6139.

(27) Clearfield, A., Tripathi, A., Medvedev, D., Celestian, A.J., Parise, J.B. *J of Mater. Sci.* **2006**, *41*, 1325-1333.

(28) Medvedev, D. G., Tripathi, A., Clearfield, A., Celestian, A.J., Parise, J.B. *Chem. Mater.* **2004**, *16*, 3659-3666.

(29) Clearfield, A., Borton, L.N., Borton, A.I. *React. and Func. Polymers* **2000**, *43*, 85-95.

(30) Bortun, A. I.; Bortun, L. N.; Clearfield, A. *Solvent Extract. Ion Exc.* **1996**, *14*, 341-354.

(31) Tripathi, A., Medvedev, D., Nyman, M., Clearfield, A. *J of Solid State Chem*, **2003**, *175*, 72-83.

(32) Shannon, R. *Acta Crystallographica Section A* **1976**, *32*, 751-767.

(33) NSLS; Laboratory, B. N., Ed. 2008; Vol. 2008.

(34) Hammersley, A. P.; ESRF: Grenoble, 2004.

(35) Bowden, M. 1998.

(36) Larson, A. C., Von Dreele, R.B. In *LAUR 86-748*; Los Alamos National Laboratory: Los Alamos, 2004.

(37) Toby, B. H. *J of Applied Crystallography* **2001**, *34*, 210-213.

(38) Rodriguez-Carvajal, J.; CEA-CNRS: 2001.

(39) Altermatt, U. D.; Brown, I. D. *Acta Crystallographica Section A* **1987**, *43*, 125-130.

(40) Laugier, J.; Bochu, B.; ENSP/Laboratoire des Materiaux et du Genie Physique: BP 46. 38042 Saint Martin d'Heres, France.

(41) Le Bail, A.; Duroy, H.; Fourquet, J. L. *Mat. Res. Bull.* **1988**, *23*, 447-452.

(42) Thompson, P.; Cox, D. E.; Hastings, J. B. *J of Applied Crystallography* **1987**, *20*, 79-83.

(43) Momma, K.; Izumi, F. In *VESTA*; 1.0.1b ed. 2007.

(44) Wills, A. S.; Brown, I. D.; v.1.0 ed.; VaList, CEA: France, 1999.

(45) Wang, H.-W.; Bish, D. L. *American Mineralogist* **2008**, *93*, 1191-1194.